Excimer laser crystallization of quasicrystalline coatings on engineering substrates

by

Arun Sadhu Kumar

A thesis submitted to the graduate faculty

in partial fulfillment of the requirements for the degree of

MASTER OF SCIENCE

Major: Mechanical Engineering

Program of Study Committee:
Pal A. Molian, Major Professor
Abhijit Chandra
Dan Sordelet

Iowa State University
Ames, Iowa
2006

Copyright © Arun Sadhu Kumar, 2006. All rights reserved.

Graduate College
Iowa State University

This is to certify that the master's thesis of

Arun Sadhu Kumar

has met the thesis requirements of Iowa State University

Signatures have been redacted for privacy

TABLE OF CONTENTS

Chapter 1. Introduction

Laser surface treatment of thin films and coatings for the purpose of converting amorphous to crystalline structures is a growing industrial application. For example, excimer laser -induced crystallization of amorphous silicon to crystalline polysilicon is a key technology for high performance thin film transistor (TFT) devices, offering excellent resolution and brightness. In this process, a 308-nm wavelength laser light is scanned across the amorphous silicon surface, as shown in Figure 1, causing efficient absorption of energy in the amorphous layer without heating the underlying substrate. During the laser pulse duration (25 ns) the amorphous-silicon layer is rapidly heated and melted. Subsequent cooling enabled the recrystallization of amorphous silicon into polysilicon.

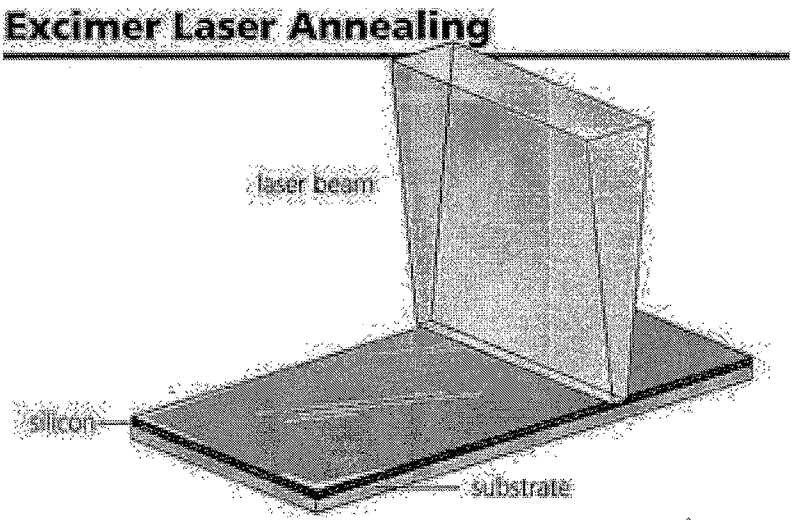

Figure 1. Schematic of excimer laser annealing with line beam optics (Source: Lambda Physik, Fort Lauderdale, FL)

Excimer Lasers

Excimer lasers are the most powerful and versatile light sources in the ultraviolet (UV) range of the electromagnetic spectrum. Excimer lasers utilize rare-halogen gas combinations (ArF,

KrF, XeCl) as light emission media and offer superior performance in the microprocessing of semiconductor and medical devices. The short and intense UV light pulses are used for numerous applications (micromachining, precise marking, and surface treatment) in the scientific, industrial and medical fields. These UV lasers are capable of producing finer features, stronger interactions with most materials, and minimal thermal damage compared to the infrared Nd:YAG and CO_2 lasers. Due to several mass production techniques based on excimer lasers becoming available, it is not surprising that these lasers represent one of the fastest growing tools in manufacturing.

Excimer Laser Annealing

Excimer Laser Annealing (ELA) is proven to be flexible and more economical than traditional furnace annealing [2]. The benefits of ELA are several, the most important one being able to control the depth of heat penetration by rapid heating (melting) and cooling of the substrate. Due to the absence of thermal effects in the underlying substrate, it becomes possible to use any type of substrate. One commercial application of the excimer laser relevant to the present work is AMLCD manufacture where silicon thin films are vapor-deposited on a glass substrate to form TFTs that control individual pixel operation [1]. However, these films exhibit amorphous structures, which must be transformed into polycrystalline in order to provide the requisite electrical properties (for example, carrier mobility). This phase transformation was accomplished previously by heating the thin films using an oven or infrared lamps. However, the temperature cycle damaged the underlying substrate material. This deficiency was overcome by the use of an excimer laser (308 nm) that was able to melt the silicon layer without heating the underlying substrate, allowing for a material savings of about $250 for a typical laptop computer display [1]. In addition, the

excimer laser enabled precise control of depth through which recrystallization occurs, as well as the crystalline grain size. No other laser could process such a thin layer without thermally affecting the surrounding material. A recent development in ELA is Sequential Lateral Solidification (SLS), a technique that involves an optical system, which shapes and homogenizes the laser beam for stitching illumination of a 4 mm x 15 mm recrystallization area with a mask technique [3]. The SLS process offers a significant reduction in the substrate illumination time.

Several research groups have used ELA for crystallizing various materials including Si [4], GaAs [5], Ge [6] and SiC [7]. In all these cases, the nanosecond-pulsed laser irradiation deposits energy within a locally defined surface, causing the formation of a liquid phase and leading to nucleation and growth of crystalline regions during solidification of the molten layer [8]. However, the crystallization process studied in depth [9-12] did not yield the conclusive evidence that the ELA process always involved the formation of liquid phase. However, one common observation by all these researchers is that the threshold laser fluence for melting depends on the thickness of the amorphous layer.

Quasicrystals

Quasicrystals (QC), a unique class of materials that do not follow the classical laws of crystallography, exhibit unconventional translational symmetry with atomic planes being assembled aperiodically. This symmetry is partially responsible for the unique combination of material properties including low friction, non-wetting behavior, high hardness and low thermal conductivity [13-16]. A classical example for quasicrystal is 65Al-23Cu-12Fe. These materials, however, have two challenges that must be overcome before widespread application can occur: 1) very limited ductility of bulk material which indicates that the

application by coating technology is the only viable fabrication method, and 2) QC materials can only be formed after a high-temperature (>700°C) anneal, which limits its application to materials that can withstand (without softening and mechanical property degradation) this elevated-temperature processing. For the second challenge, the only viable substrate materials for formation of QC coatings include metallic superalloys and ceramic materials. Thus, thermal annealing severely limits the applications of this unique coating material, unless novel processing methods can be developed.

Research Goals

In this work, the laser crystallization of the amorphous quasicrystalline thin films deposited by magnetron sputtering on aluminum, steel, and titanium substrates was investigated using a 248-nm excimer laser. The following were the objectives:

1) To justify the selection of excimer laser based on the optical properties of the film and pulse width.
2) To determine the effect of laser glazing on the crystallographic properties and the mechanical properties of the crystallized layers.
3) To study the laser annealing as a function of the laser fluence, pulse repetition rate and scan rate.
4) To identify the thermal phenomena associated with laser crystallization using a 2-D ANSYS finite element model of numerically solving the governing heat flow equation.

Thesis Organization

This thesis is organized into two papers and a chapter on conclusions. The first paper deals with the mechanical properties of controlled laser surface treatment of sputter-deposited QC

coatings (on Al, Ti, and bearing steel) and characterization of coatings by energy dispersive spectroscopy (EDS) for composition and X-ray diffraction for crystal structure. The second paper is an application of a finite element model to compute the temperature distribution and a discussion of the feasibility of the requirement of liquid phase formation for crystallization.

References

[1] D. Basting and H. Endert, "Excimer lasers for industrial microprocessing," The Industrial Physicist, September (1997), 40-44, American Institute of Physics

[2] J. Shida, S.Ishizaka, N.Kobayashi, and O.Kato, "Crystallization of a-Si Films by Excimer Laser Annealing Method," Japan Steel Works Technical Review (1997)

[3] James S. Im, "Sequential Lateral Solidification," Phy. Sta. Sol., A 166, (1998), 603

[4] J.S. Williams, and H.B. Harrison, in: J.F. Gibbons, L.D. Hess, and I.W. Sigmon (Eds.), "Laser and Electron-Beam Solid Interactions and Materials Processing," North-Holland, Amsterdam, (1981), 209.

[5] W. Wesch and G. Götz, "Rapid Annealing of ion-implanted GaAs," Phys. Stat. Sol., A 94 (1986), 745–765.

[6] F. Vega, J. Solis, J. Siegel and C.N. Afonso, "Delayed melting at the substrate interface of amorphous Ge films partially melted with nanosecond laser pulses," J. Appl. Phys. 88, 11 (2000), 6321–6326.

[7] A. Hedler, S. Urban, F. Falk, H. Hobert, and W. Wesch, "Excimer laser crystallization of amorphous silicon carbide produced by ion implantation," Applied Surface Science 205 (2003) 240-248

[8] P. Baeri, C. Spinella and R. Reitano, "Fast melting of amorphous silicon carbide induced by nanosecond laser pulse," Int. J. Thermophys. 20, 4 (1999), 1211–1221.

[9] D. Sands, P.H. Key, M. Schlaf, C.D. Walton, C.J. Anthony and M.J. Uren, "Optical characterization of lattice damage and recovery in ion-implanted and pulsed excimer laser irradiated 4H-SiC," Mater. Sci. Forum, 338–342 (2000), 655–658

[10] P.H. Key, D. Sands, M. Schlaf, C.D. Walton, C.J. Anthony, K.M. Brunson, and M.J. Uren, "Infra-red reflectivity of ion-implanted and pulsed excimer laser irradiated 4H-SiC," Thin Solid Films 364 (2000), 200–203.

[11] Y. Hishida, M. Watanabe, K. Nakashima and O. Eryu, "Excimer laser annealing of ion-implanted 6H-silicon carbide," Mater. Sci. Forum, 338–342 (2000), 873–876.

[12] H. Hobert, H.H. Dunken, S. Urban, F. Falk and H. Stafast, "Laser-induced changes of silicon carbon films studied by vibrational spectroscopy," Vibrat. Spectrosc., 29 (2002), 177–182.

[13] S. Kang, S. Dubois, and J. von Stebut, "Tribological properties of quasicrystalline coatings," J. Mater. Res. Vol. 8, No. 10, Oct. 93, 2471-2481.

[14] J.M. Dubois, P. Plaindoux, E. Belin-Ferre, N. Tamura, and D.J. Sordelet, in T. Fujiwara (Ed.), "Quasicrystals, Proc. of 6th Intl. Congress On Quasicrystals," Tokyo, Japan 1997, World Scientific, Singapore, 1998, p. 733.

[15] D. Sordelet, M. Besser, and J. Logsdon, "Abrasive wear behavior of Al-Cu-Fe quasicrystalline composite coatings," Mater. Sci. Eng. A, 1998, 255, 54-65.

[16] P. Archambault and C. Janot, "Thermal Conductivity of Quasicrystals and Associated Processes," MRS Bulletin, Nov. 1997, 48-53.

Chapter 2. Laser Crystallization of Amorphous Sputter-deposited Quasicrystalline Coatings

A paper published in "Surface and Coatings Technology," 188– 189 (2004) 274–280

F. Kustas

Engineered Coatings, Inc.

P.O. Box 4702, Parker CO 80134-4702

P. Molian, A. Sadhu Kumar

Iowa State University, Ames IA

M. Besser, D. Sordelet

Department of Energy Ames Laboratory

Ames IA

Abstract:

Quasicrystalline (QC) (e.g., $Al_{70}Fe_{10}Cu_{10}Cr_{10}$) materials offer a unique combination of relatively high hardness, low surface energy/low friction, and low thermal conductivity. This desirable suite of properties is reportedly due to their non-conventional translational symmetry and aperiodic atomic ordering. These materials can be formed only after a high temperature (>700°C) anneal and they exhibit brittle behavior in bulk form. Coating deposition alleviates the low toughness issue, but the requirement for a high-temperature anneal degrades the mechanical properties of conventional engineering substrates. To address this latter issue, controlled laser surface treatment of sputter-deposited QC coatings

(on Al, Ti, and bearing steel alloys) was performed to convert the amorphous (a) structure into a crystalline (c) phase. Characterization of both a-QC and c-QC films included Energy Dispersive Spectroscopy and x-ray diffraction for composition/structure, C-brale indentation for relative toughness, and ball-on-disk (BOD) friction / wear tests. Laser treatment was successful in converting the amorphous structure to the crystalline phase, without significant reduction (<10% for Ti-6Al-4V) in substrate hardness, and it was shown that laser pulse energy influences the final surface finish of the c-QC surface. Laser crystallization was observed to increase the indentation resistance / adhesion of c-QC films on coated Ti-6Al-4V and 52100 steel. Friction / wear tests of c-QC films showed reductions in coefficients of friction, compared to non-coated substrates, of ~40%, ~20-25%, and ~25-30%, respectively, for coated 2024-T3Al, Ti-6Al-4V, and 52100 steel substrates. Reductions in wear damage for c-QC coated surfaces, compared to non-coated surfaces, were also observed.

Keywords: Quasicrystalline coatings; Sputtering; Laser crystallization; Friction/wear; Indendation

1. Introduction

Quasicrystals (QC) (e.g., Al_{65}-Cu_{23}-Fe_{12}), exhibit a unique combination of material properties, such as: 1) low surface energy, low friction (0.07-0.23 [1]), and non-wetting behavior, due to a reduced density of states at the Fermi energy [2], 2) high hardness (up to 8.1 GPa [3]) from aperiodic atomic ordering which interrupts dislocation movement, and 3) low thermal conductivity, ~ 1.8 W/m°K [4] for Al-Cu-Fe. Materials with this unique set of properties are excellent candidates for tribological systems (e.g., engine components such as piston rings, cylinder liners, gears, and bearings) that require low-friction, wear-resistant

insulating surfaces. These materials, however, have two limitations that must be addressed before widespread application will occur: 1) QC materials can only be formed after a high temperature (≥700°C) anneal, which limits its application to materials that can withstand this elevated-temperature processing and 2) very limited ductility of bulk material which suggests application by coating technology is the only viable fabrication method. The first limitation has severely restricted application of QC coatings to mostly deposition by thermal or plasma spray methods. If the technology could be developed to fabricate QC coatings on more conventional engineering alloys, such as aluminum (Al), titanium (Ti), and bearing steel alloys, then more applications would result.

In this program , we investigated an alternate thermal processing method, laser treatment to convert as-sputtered amorphous (a)/nanocrystalline coatings to the crystalline phase.

2. Experimental

2.1. Substrate Materials

Conventional engineering materials 2024-T3 Al, annealed Ti-6Al-4V, and quenched and tempered (Q&T) 52100 steel disk coupons (2.54 cm (1.0 in.) and 1.91 cm (0.75 in.) diameters x 0.64 cm (0.25 in.) thick) were used in this study. Profilometry was performed to establish a roughness average (R_a) baseline of the lapped surfaces, for comparison with as sputtered and sputtered & laser treated coupons. Average R_a values for the lapped coupons were: 1) 2024-T3 Al: 0.066 μm (2.60 μin), 2) Ti-6Al-4V: 0.076 μm (2.99 μin), and 3) 52100: 0.047 μm (1.85 μin). In general, these values are actually finer than most machined parts used in engine applications.

2.2. Fabrication of Quasicrystalline Sputtering Targets

DOE-Ames Laboratory fabricated QC sputter targets by plasma-spraying atomized powder onto copper backing plates. Composition analysis, by Energy Dispersive Spectroscopy (EDS), verified that the target composition was close to the goal of $Al_{70}Fe_{10}Cu_{10}Cr_{10}$.

2.3. Physical Vapor Sputter Deposition of Amorphous Quasicrystalline Coatings

A standard substrate cleaning protocol was applied to the metal coupons prior to coating. Immediately prior to deposition, a plasma-etch (typically at a voltage of >500V) was performed to remove any further contamination and oxides. For all of the depositions, a Ti bond layer (~150 nm (5.9 μin thick)) was applied by unbalanced-magnetron (UBM) direct current sputtering to facilitate adhesion of the a-QC coatings to the metal substrates.

Unbalanced magnetron sputter depositions of a-QC coatings onto the engineering substrates were performed to different coating thicknesses (Table 1), with thicker films (>12 μm (472.4 μin)) being prepared for structure and composition analysis, and thinner films (e.g., 5 μm (196.9 μin) and 2.5 μm (98.4 μin)) for mechanical and tribological property tests. As observed in Table 1, all depositions were performed at a nominal Ar working gas pressure of 0.33 Pa. A moderate temperature ~125°C (257°F) thermal bake-out of the substrates during deposition, to remove any excess water vapor from the surfaces, was also investigated. We previously observed this treatment to be beneficial for increasing coating adhesion. Quasicrystalline coating depositions were performed with a low bias (e.g., -20V) as from previous work it was shown that coating composition was closer to the target composition under low-bias deposition conditions [5].

2.4. Spectral Reflectance Measurements on Amorphous Quasicrsytalline Coatings

To assist in selection of the most appropriate laser for processing, as-sputtered a-QC coatings (on 2024-T3 Al, Ti-6Al-4V, and 52100 steel) were scanned using a LAMBDA19 Reflectance Spectrometer to provide coating spectral reflectance. This device measures reflectance, as a function of wavelength, over the normal solar spectrum from 0.2 μm-2.5 μm, which is characteristic of most available lasers. In general, for best coupling with a laser device, a low reflectance (or high absorptance) is desired.

2.5. Laser Surface Treatments

Laser treatments using an excimer system of ~1/2 of each coated disk were conducted to enable a study of laser pulse power on surface roughness and crystallization of the a-QC films. Laser pulse power levels applied were: 1) 50 and 100 mJ for 2024-T3Al, 2) 56 and 112 mJ for both Ti-6Al-4V and 52100 steel, and 3) 10-200 mJ for 2024-T3Al in the surface roughness study. Laser parameters that were held constant for all of the laser processing trials included: 1) repetition rate: 40 Hz, 2) spot size: 2 mm x 1 mm, 3) table speed: 1.27 cm/sec, and 4) beam overlap: 5%. After an iteration in laser parameters and surface characterization, processing of entire sputter-coated surfaces was performed to provide substrates for mechanical and tribological tests.

2.6. Coating Characterization and Testing

Several characterization and testing techniques were used to determine the performance of as-sputtered and sputtered & laser-treated QC coatings. Surface roughness and coating thickness measurements were performed by diamond stylus profilometry on as-lapped non-coated substrates, sputter-coated a-QC films, and sputter-coated & laser-treated QC films. Microstructure (i.e., amorphous or crystalline phases) of as-sputtered and as-sputtered &

laser-treated QC coatings was determined by performing normal incidence Θ–2Θ x-ray diffraction analyses on selected coatings.

Mechanical properties were measured on the as-sputtered and sputtered & laser-treated QC coatings. Indentation using a Rockwell hardness tester with a conical "C-Brale" indenter was performed to investigate coating adhesion and coating/substrate relative toughness, cracking behavior, and also to quantify bulk hardness after laser treatment. This method has been used as a standard method to rank coating adhesion by comparing the indentation behavior with a set of characteristic cracking and flaking patterns [6]. In addition, this method can also used to compare coating / substrate interfacial toughness (K_{1i}) [7] for coatings prepared by different parameters by a comparison of the slopes of the lateral crack length vs. indentation load functions. Ball-on-disk (BOD) friction / wear tests were performed to provide both resisting frictional force (which was subsequently converted to coefficient of friction (COF)) and wear scars for photographic characterization. Different ball materials, such as hardened Cr-steel (HRC 60), silicon nitride, and tungsten carbide were used in the wear tests. An analytical expression for a ball-on-flat contact was used to calculate the initial contact stress. Tests were conducted under non-lubricated conditions in room-temperature air and at a relative sliding speed of 2.54 mm/sec (0.1 in/sec). Table 2 lists the parameters that were used for the wear tests.

3. Results and Discussion

3.1. Spectral Reflectance Measurements

For all of the coated substrates, reflectance values were relatively high (e.g., ~55% for bearing steel and ~72% for Ti alloy) at the starting wavelength of 0.2 μm. With increasing

wavelength, reflectance dropped to a minimum and then increased again at higher wavelengths. Minimum reflectance values and wavelengths for the coated substrates were: 1) 52100 steel: 37% at 250 nm, 2) Al alloy: 25% over ~350-550 nm, and 3) Ti alloy: ~48% at 500 nm. For the coated bearing steel, it appears a KrF excimer laser, with a wavelength of 248 nm, is almost a perfect fit. For the coated Al substrate, it appears the frequency-doubled Nd:YAG laser, with a wavelength of 532 nm, is the best fit. However, the reflectance difference between 248 and 532 nm is quite small (e.g., ~27-28% reflectance at 248 nm vs. ~25% reflectance at 532 nm), therefore the excimer device would also be a good selection. The a-QC coated Ti alloy exhibited a similar behavior with reflectance at 248 nm being only slightly higher (e.g., ~52-53% reflectance) than the reflectance at 532 nm (~47-48%). Therefore a KrF excimer laser is recommended for processing of QC-coated 52100 steel, while either the excimer or the Nd:YAG could be used for QC-coated Al and Ti alloy substrates. We subsequently selected an excimer laser for this study, since an operational system was readily available.

3.2. Surface Roughness

Table 3 lists the roughness average (R_a) measurements on as-lapped substrates, sputter-coated a-QC films, and laser-treated QC films. As-lapped substrates exhibited very smooth surfaces, less than 0.076 μm (3 μin) R_a. For as-sputtered a-QC coatings, increased roughness was measured, with up to a 27% increase in R_a. However, these values are still very small, presumably from the lapping treatment applied to the underlying substrates. For laser-treated coatings (which were also thicker) increases in roughness were measured and for 2 of the 3 specimen sets (the exception being Ti-6Al-4V), higher roughness was observed for higher-energy laser treatment. However, once again the absolute values of roughness were not

extremely high, with a maximum R_a of about 0.516 μm (20.3 μin). The larger values of R_a observed for the laser-treated QC coatings may also be influenced by the greater thickness of the as-sputtered a-QC coatings.

An a-QC sputtered-coated 2024-T3 Al was subjected to a series of laser treatments at different pulse energy levels, to investigate effects of laser energy on surface roughness. A general trend of increasing roughness with increased laser energy level was observed and there was a distinct jump in R_a between the energy levels 75 mJ (0.24 μm) and 100 mJ (0.44 μm). Since it was observed that nearly the same crystalline XRD spectra was found for either a 50 or 100 mJ treatment on a QC coated 2024-T3 Al specimen (next section), the lower energy level was determined to be sufficient to crystallize the a-QC coating and also reduce the roughening from laser processing.

3.3. Composition and Microstructure

Energy dispersive spectroscopy was performed on a sputter-coated & laser treated QC coating to investigate any composition differences from the QC sputter target. As shown in Table 4, a slight enrichment in Cr and decrease in Fe (from the goal composition) was measured for the starting plasma-sprayed sputter target. In contrast, after sputtering and laser-treatment, there was a slight increase in Al and Cu, with a slight decrease in Fe content.

X-ray diffraction analysis was performed on as-sputtered and sputtered & laser-treated QC coatings on all 3 engineering substrates. An example of the structural evolution from amorphous QC (sputtered film) to a crystalline QC structure (after laser treatment) is shown in Figure 1 for coatings on 52100 steel. From Figure 1, there is an underlying main peak for the 52100 steel substrate at ~44.7°, which was hidden under the broadened spectra for the a-QC sputtered coatings, and not observed for the laser treated coatings. Discrete crystalline

peaks (marked with asterisks), separate from the amorphous peak, were observed for laser treatments A and B. The highest intensity peaks, located at ~42, 44, 23, and 27 degrees all appear to be characteristic of the stable icosahedral phase, as reported in Ref. [5]. However Dubois et al [8], describe a large number of possible structures for Al-Cu-Fe-Cr phases, including a polymorphous approximant, O2 to the decagonal phase with an orthorhombic structure, which has an atomic composition that is fairly close (i.e., $Al_{68.6}Cu_{8.2}Fe_{10.7}Cr_{12.5}$) to the bulk composition of the crystallized QC films fabricated in this study. The microstructure evolution shown in Figure 1 for 52100 steel is similar to that observed for coatings on 2024-T3 Al and Ti-6Al-4V, with broadened amorphous peaks for the as-sputtered QC coatings and discrete crystalline peaks for the laser-treated coatings. Therefore regardless of the substrate material, it was possible to crystallize the sputter-deposited amorphous QC coating using low-pulse power (e.g., 50-56 mJ) excimer laser treatment.

3.4. Rockwell C-Brale Indentations

Rockwell hardness measurements were made on laser-treated QC coatings to determine if the localized high-temperature laser treatment reduced the bulk hardness of the substrates. From the measured hardness data, laser surface treatment did not temper or reduce the bulk hardness of the 2024-T3 Al or 52100 steel substrates. However, for the Ti alloy, there was a slight softening of about 10% (from HRC of ~34 to ~30) for the surface with the laser treated QC coating. Examination of the Rockwell C-Brale indentations, applied at different loads, was also performed to examine coating adhesion and cracking resistance from tensile-loading at the indent/coating interface. For moderately thick (5 μm) a-QC coatings on 52100 steel and the Ti alloy, widespread coating flaking and cracking (e.g., Figure 2a for 52100 steel) was observed. This might be due to the production of higher residual stress for the thicker

coatings and poor adhesion to the steel and Ti alloy substrates. In contrast, the a-QC coated 2024-T3Al substrate only experienced radial cracking, however, at the highest load of 150 kg some localized minor flaking was also observed. This improved adhesion of the a-QC coating to the Al alloy substrate may be due to the high concentration of Al in the QC coating composition, increasing the compatibility between the coating and the Al alloy substrate. In an effort to increase a-QC coating adhesion, a moderate (i.e., ~125°C) thermal treatment was applied to the substrates prior to and during sputter deposition to drive off any surface contaminants (e.g., water vapor). In addition, coating thickness was reduced (to 2.5 μm) to reduce coating residual stress. This thermal processing (along with the reduced coating thickness) successful improved adhesion of the a-QC coatings and reduced cracking/flaking damage from indentation, (e.g., Figure 2b), and was used for subsequent sputter depositions for industry trials evaluations (Table 1).

Laser treatment increased the cracking/flaking resistance to indentation for thick (e.g., 12.7 μm) sputtered a-QC coatings on 52100 steel (no measurable flaking was observed, see Figure 3 for #341) and reduced the extent of flaking for QC-coated Ti-6Al-4V (at the higher applied load of 150 kg). For the laser treated QC/Al substrate, well-defined flaked diameters were measured, which were larger than the radial cracking pattern measured for the a-QC coated Al substrate. Note also the undulations near the indent in Figure 3, due to the pulsing of the laser beam during crystallization processing. These benefits in adhesion were observed for much thicker c-QC coatings (i.e., 12.7 μm (#341)) that were deposited on non-heated metal substrates. This suggests that laser surface treatment may even further improve coating adhesion/toughness on thinner coatings applied to heated substrates.

3.5. Friction / Wear Performance

For all of the crystallized c-QC coatings, average COF values vs. mating Cr-steel (and vs. Si_3N_4) were reduced, for example ~25-30% for c-QC coated steel, ~40% for c-QC coated Al alloy, and ~20-25% for c-QC coated Ti alloy.

3.5.1. 52100 Steel Substrate

Coefficient of friction for noncoated 52100 steel (vs. Cr-steel) exhibited a continually increasing and erratic COF with time (Figure 4a). The wear scar showed evidence of wear debris (Figure 4b), possibly due to stick-slip wear behavior. In contrast, laser-treated c-QC coating #347 exhibited a reduced COF by about 25-30% vs. Cr-steel and an even larger reduction of ~60% vs. Si_3N_4 to a COF<0.2. The wear scar for laser treated c-QC coated 52100 steel (vs. Cr-steel), appeared "smeared or polished" (Figure 4c), without evidence of transferred material from the mating Cr steel ball. Steel [1] and stainless steel alloys [9] have been previously coated with QC alloys by high-temperature flame spraying [1], supersonic spraying [1], plasma spraying [1], and RF magnetron sputtering followed by annealing [9]. For a quaternary alloy of similar composition (but slightly higher Cu) to our films, a friction value of about 0.22 was reported for a thick (e.g. 60 μm) flame-sprayed QC coating on low-carbon steel vs. a hard steel indenter [1], which is lower than our measured value of about 0.31 (Figure 4). However, it was shown (in Ref. [1]) that COF is reduced for thicker films and by interpolation of their COF data, our COF value was comparable to their value of 0.29 for a 10μm flame-sprayed QC coating. Our observation of reduced COF for harder counterface materials (e.g.,Si_3N_4) also follows the trend reported in Ref. [1] with lower COF for a diamond stylus, compared to steel.

3.5.2. 2024-T3Al Substrate

Coefficient of friction for bare 2024-T3Al (vs. Cr-steel) showed a very erratic COF behavior, again suggestive of stick-slip wear, while COF for the laser-treated QC coating #347 exhibited much less scatter and achieved about a 40% lower equilibrium value. Wear scars, showed much less wear scar damage for the laser-treated c-QC coating, even at the high initial contact stress which was greater than the compressive yield strength of the Al alloy. At a lower initial stress (below the compressive yield strength of 2024-T3Al) of 361.3 MPa (52.4 ksi), very minor wear damage was observed for the laser-treated c-QC coating, while wear damage to the bare Al substrate was still considerable. From ref. 1, supersonic spraying of a thick (again 60 μm) ternary $Al_{65}Cu_{20}Fe_{15}$ alloy onto an Al alloy exhibited a COF of about 0.19 vs. a hard steel counterface, which is again lower than our average measured COF of about 0.4. A similar trend of higher COF for thinner supersonic sprayed films on the Al alloy was reported [1].

3.5.3. Ti-6Al-4V Substrate

Coefficient of friction for laser treated c-QC coating #347 on Ti-6Al-4V (vs. Cr-steel) showed a trend of reduced COF with time and about a 20% lower equilibrium COF (~0.26) compared to a trend of increased COF with time for bare Ti-6Al-4V. The wear scar for the bare Ti-6Al-4V surface showed several deep grooves, while the wear scar zone appeared smoother with a reduced number of grooves for the laser treated c-QC coating #347.

4. Conclusions

Laser treatment of sputter-deposited amorphous Al-Fe-Cu-Cr films on conventional engineering substrates 2024-T3 Al, annealed Ti-6Al-4V, and hardened and tempered 52100 bearing steel was successful in crystallizing the amorphous films without significantly

degrading the bulk hardness of the underlying substrates. Surface roughness, compared to lapped metal coupons, was increased slightly for sputtered films, but considerably more for laser-crystallized films. Surface roughness can be reduced somewhat by lowering the incident laser pulse power. Moderately heating the substrates prior to and during deposition and reducing the coating thickness increased adhesion of sputter-deposited a-QC coatings. Laser treatment of thicker (e.g., 12.7 μm) a-QC coatings deposited onto non-heated substrates exhibited much improved adhesion and greater cracking/flaking resistance than thinner a-QC coatings deposited onto non-heated substrates. This suggests that laser treatment of thinner sputtered a-QC films deposited onto heated substrates may provide very good adhesion. Coefficients of friction were reduced (compared to non-coated metal substrates) by ~25-30%, ~40%, and ~20-25% for crystalline QC coatings on steel, Al alloy, and Ti alloy substrates, respectively. Wear damage within the wear scars was also modified from heavy wear debris deposits for non-coated wear couples, suggesting material transfer from the mating ball material, to a minor polishing/smearing type of wear behavior for the crystallized QC coatings.

Acknowledgements

The authors would like to acknowledge the financial support of U.S. National Science Foundation for this work, under SBIR grant SMI-0231722, "Laser Crystallization of Amorphous Sputter-Deposited Quasicrystalline Coatings on Conventional Engineering Substrates", awarded to Engineered Coating, July 2003.

References

[1] S. Kang, S. Dubois, and J. von Stebut, J. Mater. Res., 8 (10) (1993) 2471

[2] J. M. Dubois, P. Plaindoux, E. Belin-Ferre, N. Tamura, and D. J. Sordelet in T. Fujiwara (ed.) Quasicrystals, Proc. of 6th Intl. Congr. On Quasicrystals, Tokyo, Japan 1997, World Scientific, Singapore 1998, p 733

[3] D. Sordelet, M. Besser, and J. Logsdon, Mater. Sci. Eng., A 255 (1998) 54

[4] P. Archambault and C. Janot, MRS Bulletin, (1997) 48

[5] D. J. Sordelet, M. Besser, and F. Kustas, Mat. Res. Soc. Symp. Vol. 643, Materials Research Society, 2001

[6] W.-D. Munz et al, J. Vac. Sci. Technol., A 11 (5) (1993) 2583

[7] P. Jindal et al., Thin Solid Films, 154 (1987) 361

[8] J. M. Dubois, et al, Ann. Chim. Fr. 19 (1994) 3

[9] Y. Ding, D. Northwood, A. Alpas, Surface and Coatings Technology 96 (1997) 14

List of Tables

Table 1

Summary of sputter coating depositions

Coating number	Substrate heating	Target thickness, μm	Substrates coated
341	No	7.5	2.54 cm diameter 2024-T3Al, Ti-6Al-4V annealed, 52100 Q&T, TEM Cu grids (2)
342	No	7.5; measured: 12.66	2.54 cm diameter 2024-T3Al, Ti-6Al-4V annealed, 52100 Q&T, SS strip
343	No	~12.66	2.54 cm diameter 2024-T3Al, Ti-6Al-4V annealed, 52100 Q&T
344	No	~5	2.54 cm diameter 2024-T3Al, Ti-6Al-4V annealed, 52100
347	Yes, ~125°C	~2.5	2.54 cm diameter 2024-T3Al; 1.91 cm diameter Ti-6Al-4V annealed, 52100 Q&T
352	Yes, ~125°C	~2.5	2.54 cm diameter 2024-T3Al; 1.91 cm diameter Ti-6Al-4V annealed, 52100 Q&T
353	Yes, ~125°C	~2.5	2.54 cm diameter 2024-T3Al; 1.91 cm diameter. Ti-6Al-4V annealed, 52100 Q&T

Table 2

Parameters for ball-on-disk friction/wear tests

Ball material, diameter, mm (in)	Substrate and condition	Applied load, N (Lb)	Initial stress, MPa (ksi)
Cr-steel (HRC60) 4.0 (0.16)	2024-T3Al; bare & coated	1.25 (0.28)	495.8 (71.9)
	2024-T3Al; bare & coated	3.0 (0.68)	661.9 (96.0)
Cr-steel (HRC60) 6.4 (0.25)	2024-T3Al; bare & coated	1.25 (0.28)	363.4 (52.7)
Cr-steel (HRC60) 4.0 (0.16)	Ti-6Al-4V; bare & coated	5.62 (1.26)	992.9 (144)
Cr-steel (HRC60) 4.0 (0.16)	52100; bare & coated	6.53 (1.47)	1,289.4 (187)
WC-Co, 4.0 (0.16)	52100; bare & coated	11.2 (2.51)	1,965.1 (285)
	52100; bare & coated	3.1 (0.70))	1,289.4 (187)
Si_3N_4 4.0 (0.16)	coated 52100	6.5 (1.46)	1,289.4 (187)

Note: Wear scar diameter and rotational rate adjusted to provide constant sliding speed of 2.54 mm/sec (0.10 in/sec).

Table 3

Summary of roughness average values for as-lapped, sputter-coated, and laser treated QC coatings showing some roughening from laser processing

Substrate	Coating number	Coating thickness, μm	Laser treatment	Roughness average, μm	μin	% Change from bare substrate
2024-T3 Al	None	None	None	0.0659	2.6	—
2024-T3 Al	347	~2.5	None	0.0819	3.2	+24.3
2024-T3 Al	341	~12.7	A: 50 mJ	0.2262	8.9	+243.4
2024-T3 Al	341	~12.7	B: 100 mJ	0.5163	20.3	+683.9
Ti-6Al-4V annealed	None	None	None	0.0761	3.0	—
Ti-6Al-4V annealed	347	~2.5	None	0.0963	3.79	+26.6
Ti-6Al-4V annealed	341	~12.7	A: 56 mJ	0.4502	17.7	+491.8
Ti-6Al-4V annealed	341	~12.7	B: 112 mJ	0.3919	15.4	+415.1
52100, Q&T	None	None	None	0.0469	1.9	—
52100, Q&T	347	~2.5	None	0.0436	1.7	-7.2
52100, Q&T	341	~12.7	A: 56 mJ	0.2647	10.4	+464.0
52100, Q&T	341	~12.7	B: 112 mJ	0.4520	17.8	+863.1

Table 4

Composition analysis by energy dispersive spectroscopy of QC sputter target and sputtered & laser treated QC coating showing minor composition differences.

Condition	Coating composition, at.%			
	Al	Cr	Fe	Cu
Target goal	70	10	10	10
Plasma sprayed sputter target	69.8	11.2	8.9	10.1
Sputtered and laser treated QC coating	71.5	9.8	8.0	10.7

List of Figures

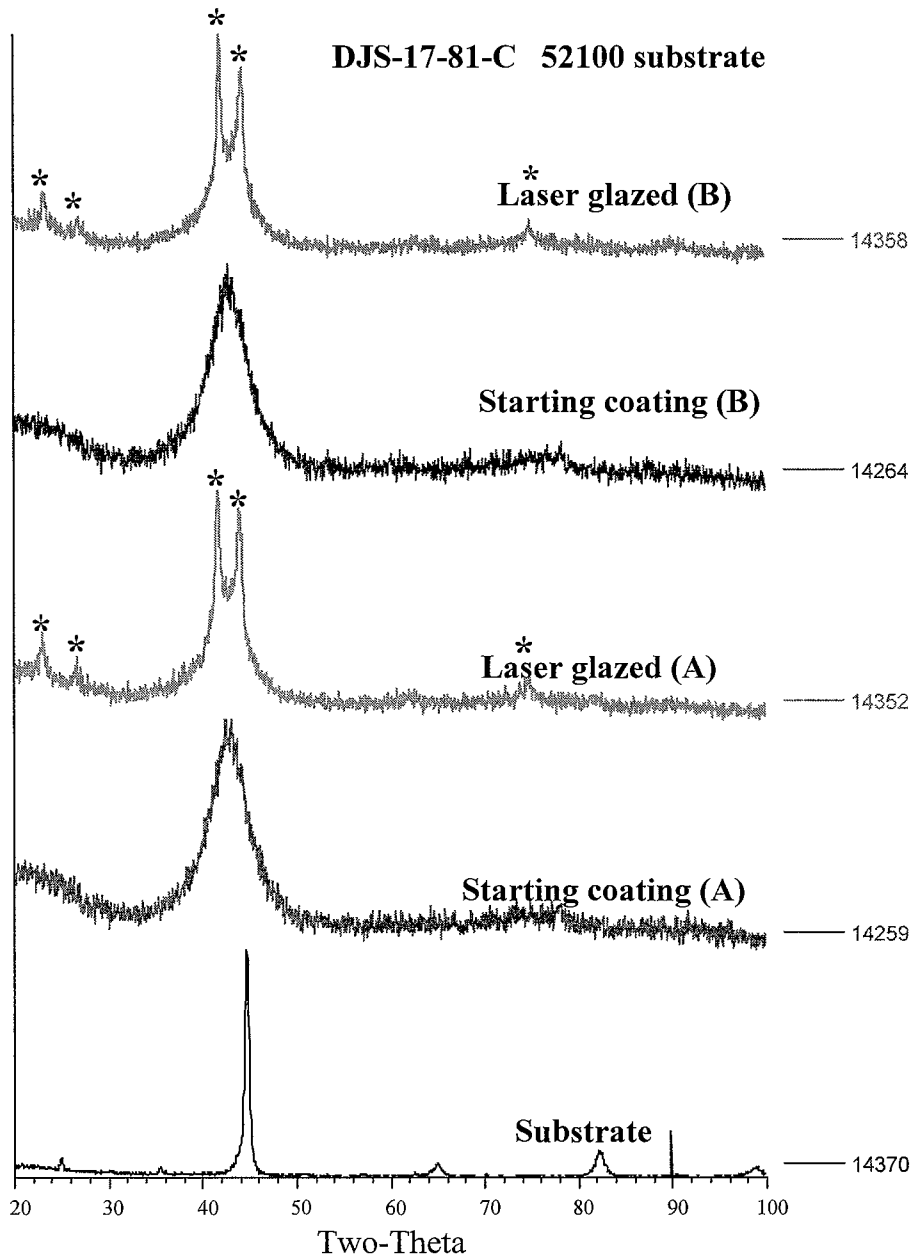
DJS-17-81-C 52100 substrate
Laser glazed (B)
14358
Starting coating (B)
14264
Laser glazed (A)
14352
Starting coating (A)
14259
Substrate
14370
20
30
40
50
60
70
80
90
100
Two-Theta

Figure 1

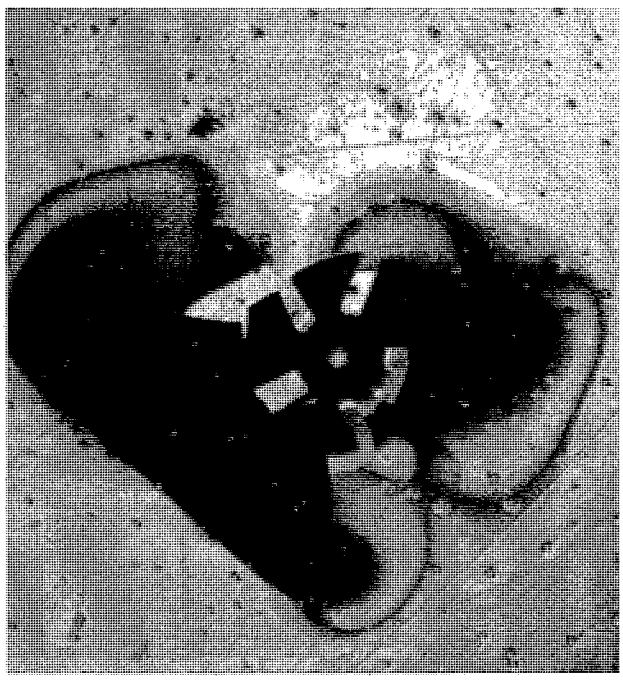

a)

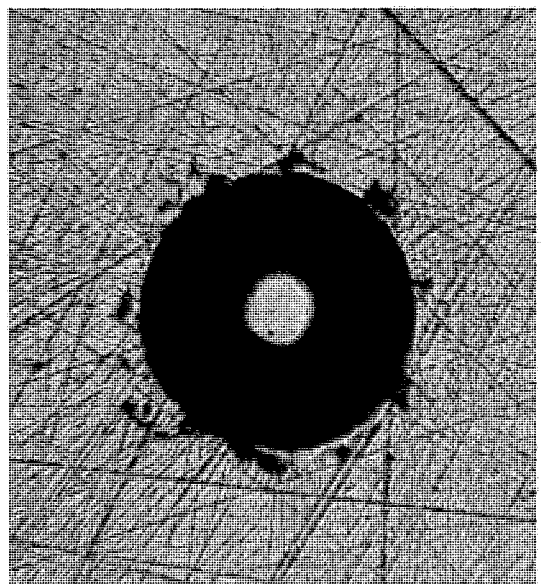

b)

Figure 2

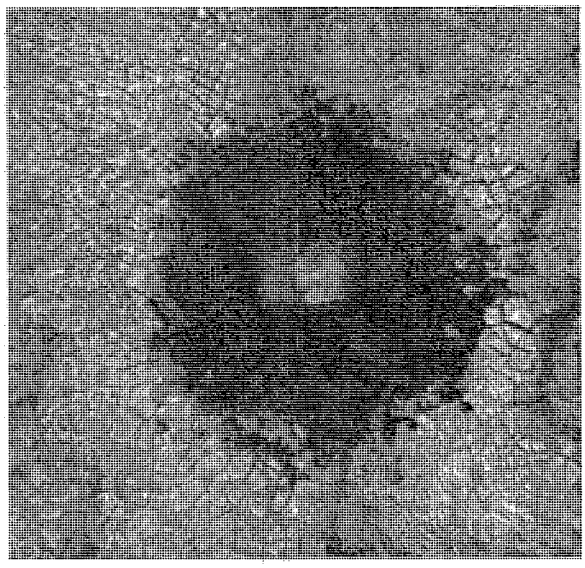

Figure 3

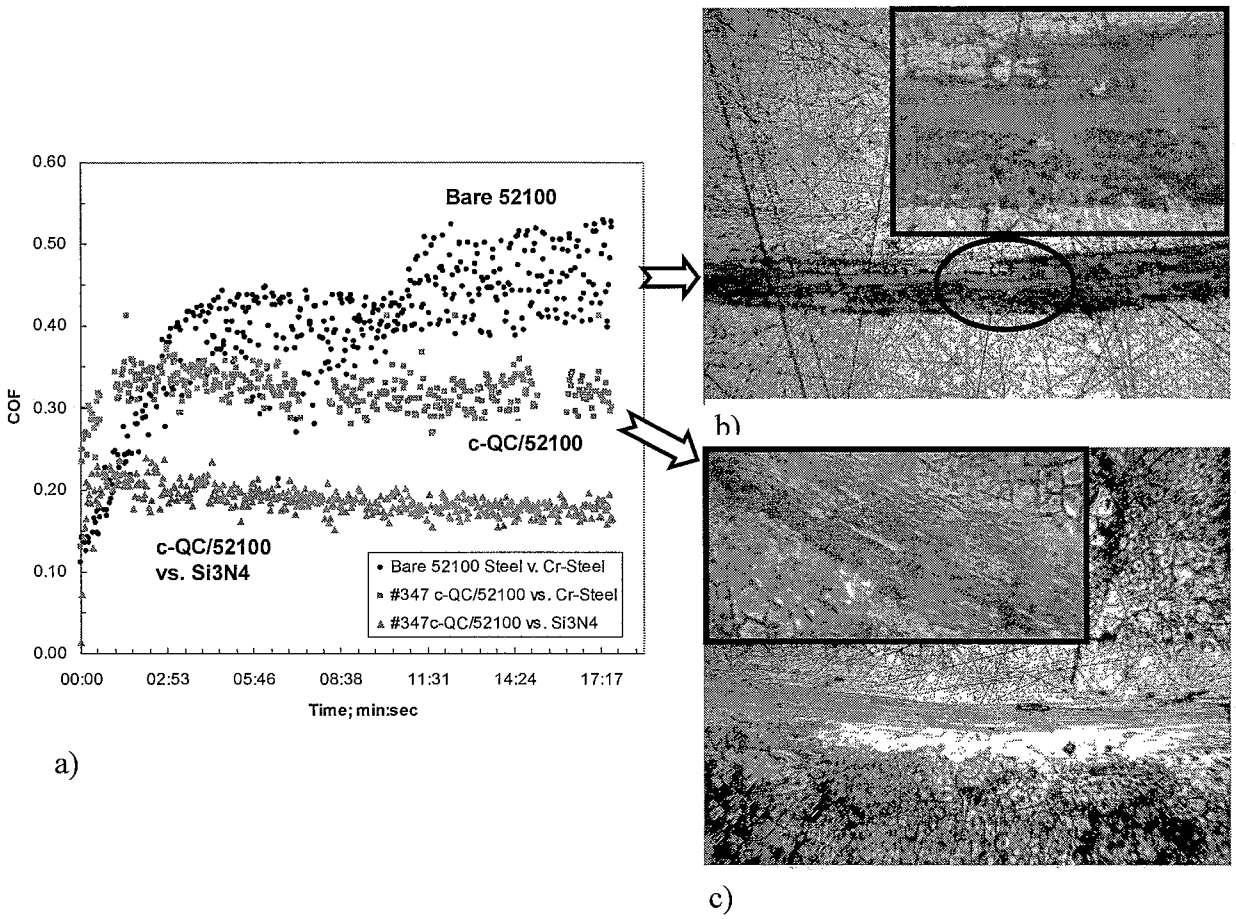
0.60
0.50
0.40
0.30
0.20
0.10
0.00
COF
Bare 52100
c-QC/52100
c-QC/52100
vs. Si3N4
• Bare 52100 Steel v. Cr-Steel
▫ #347 c-QC/52100 vs. Cr-Steel
▵ #347c-QC/52100 vs. Si3N4
00:00
02:53
05:46
08:38
11:31
14:24
17:17
Time; min:sec
a)
b)
c)

Figure 4

Chapter 3. Excimer Laser Annealing of Quasicrystalline Coatings

A. Sadhu Kumar* and P. A. Molian

Department of Mechanical Engineering, Iowa State University, Ames, IA 50011-2161

A paper submitted to Lasers in Engineering

Abstract

Excimer laser annealing (ELA) is well known to cause the transformation of amorphous to crystalline structures in semiconductor materials such as silicon and germanium. However, there exists a disagreement on whether this phase transition involves formation of liquid phase or takes place exclusively in solid-state. In this work, ELA of amorphous 65Al-23Cu-12Fe quasicrystalline (QC) coatings was performed to elucidate the mechanism of phase transition. Magnetron sputtering was used to deposit 10 to 12 μm thick amorphous QC coatings on steel, aluminum and titanium substrates followed by ELA to convert them into crystalline phases. X-ray diffraction data of ELA samples was used to determine the threshold energy fluence for phase transformation. A two-dimensional, finite-element thermal model was applied to estimate the temperature distributions and melt depth as a function of energy fluence. The effect of ELA on surface roughness was measured and also used to identify the phase change. Results infer that ELA caused the melting of about 3 μm layer of the coating at threshold fluence and more at higher energy fluences. Surface roughness (arithmetic average) was increased from an average of 0.06 μm in as magnetron-sputtered to 0.4 μm in laser-crystallized coatings. It is concluded that the presence of thin melt layer is a necessary and sufficient condition for the phase transition to occur and that the formation of melt layer roughens the laser-modified surface, a chief drawback of ELA.

* Corresponding Author – arunspeaks@yahoo.com

Keywords: Excimer laser, annealing, phase transition, quasicrystalline material

1. Introduction

Conventional engineering materials such as quenched and tempered steels, precipitation-hardened aluminum and titanium alloys represent the bulk of materials used for components in moving mechanical assemblies (engines and transmissions). These substrates are often coated with different materials or surface modified (shot peening, carburizing, flame and induction hardening) to improve the surface properties such as friction, wear, corrosion and fatigue resistance. An emerging coating material which shows tremendous promise for applications in industry is the quasicrystalline (QC) alloys (Al-Cu-Fe) that offer a combination of properties such as: (a) low surface energy, low friction (0.07-0.23) and non-wetting behavior, due to a reduced density of states at the Fermi energy, (b) high hardness (up to 8.1 GPa) from aperiodic atomic ordering which interrupts dislocation movement, and (c) low thermal conductivity, ~ 1.8 W/m K [1-4]. The unique characteristics of QC alloys enable them to be applied as ideal tribological and thermally insulative coatings for the engineering substrates.

QC coatings are currently applied by plasma spray and sputtering methods that tend to produce amorphous structures. In order to obtain crystalline structures, the QC coatings are subjected to annealing at or above 700°C using a furnace or arc lamp for hours. Unfortunately, these annealing methods seriously weaken the substrates through thermal degradation. For example, steel and aluminum soften due to tempering and overaging respectively, reducing their load-carrying capability as well as fatigue life. Table 1 presents

some of the thermal limitations of conventional engineering substrates, suggesting that the long-time heat-treatment of these alloys at temperatures greater than 700°C significantly reduces their properties. In an effort to overcome this problem, we have recently reported a sequential process involving magnetron

Table 1. Thermal limitations of conventional engineering alloys

Alloy	**Density, g/cm^3 (lb/in^3)**	**Tempering or Aging Temperature, °C (°F) and effects on properties**
6061-T6 Al (1.0 Mg, 0.6 Si, Al-bal.)	2.65 (0.098)	Aging: 160-177°C(320-350°F); Anneal: 413°C (775°F) 20% reduction in tensile strength at 177°C (350°F)
Ti-6Al-4V (6.0 Al, 4.0 V, Ti-bal.)	4.32 (0.16)	Aging: 482-538°C (900-1000°F); 40% reduction in yield strength at 427°C (800°F)
440 C Steel (17Cr,1C, Fe-bal)	7.56 (0.28)	Temper: 149-371°C (300-700°F); Maximum service temp ~ 427°C (800°F)

sputtering and excimer laser crystallization (Figure 1) to synthesize crystalline QC coatings on Al, Ti, and steel substrates [5]. The major findings of our study include:

1) Magnetron-sputtering produced amorphous QC coatings and subsequent laser annealing resulted in crystalline structures.

2) The underlying engineering substrates were neither tempered nor softened to significant extent (maximum hardness loss was less than 10% for Ti alloy).

3) Surface roughening was observed but a reduction in pulse energy reduced the magnitude of roughening.

4) Considerable improvement in coating adhesion and relative coating/substrate interface toughness was observed in high-load indentation tests.

5) Significant reduction in coefficients of friction and wear damage/surface adhesion were noted.

In this paper, we focus on understanding the phase transition mechanism in ELA through a three-step procedure. First, the crystallization and surface roughness of QC coatings were experimentally evaluated as a function of energy fluence through X-ray diffraction and profilometer respectively. Second, a finite-element model (FEM) was applied to predict the temperature distribution as a function of energy fluence by numerically solving the heat flow equation that governs the excimer laser-QC material interactions. Third, the FEM results in conjunction with X-ray and surface roughness data were used to predict the phase transition mechanism of excimer laser-annealed QC coatings.

2. Experimental Details

Three different substrate materials (52100 steel, 2024 aluminum and Ti-6Al-4V) were coated with QC (65Al-23Cu-12Fe) to 10-12 μm thick using unbalanced magnetron sputtering (UBMS) method. The attributes of UBMS over plasma-spray coatings are improved density, excellent adhesion, fewer defects, smoother surfaces, and lower processing temperatures that

neither temper nor overage the substrate alloys. X-ray diffraction analysis of these QC coatings revealed the presence of amorphous structures.

Following sputtering deposition, the reflectance of QC coatings was determined using a LAMBDA19 Reflectance Spectrometer as a function of wavelength. Figures 2 through 4 are the reflectance curves showing that with increasing wavelengths, the reflectance drops to minimum at a specific wavelength and then increases. Although the minimum reflectance was observed at different wavelengths for each of the coated substrates, we chose the excimer laser at a wavelength of 248-nm to treat all three substrates as it is easier to control the heat penetration depth with nanosecond pulses and UV radiation. It has also been demonstrated that UV excimer lasers are better choices than Nd:YAG (λ=1064 nm) and CO_2 (λ = 10,600 nm) lasers for annealing the coatings without damaging the underlying substrate [6-8].

Table 2. Excimer laser specifications

Medium	**Wavelength (nm)**	**Pulse Energy (mJ)**	**Repetition Rate (Hz)**	**Pulse Width (ns)**	**Beam size (mm)**
KrF	248	0-300	1-100	23	23x12

Table 2 lists the specifications of the excimer laser (Lambda Physik, Model LPX 110) used in the experiments. The 248-nm KrF excimer laser with a pulse width of 23 ns was used to irradiate the QC coatings by rastering a rectangular beam (2 mm x 1 mm) on the surface at various pulse energies (10 mJ to 200 mJ) in an inert gas (argon) environment. The pulse repetition rate was made constant at 40 Hz. The QC coated sample was mounted on an X-Y

stage which is made to move at a constant speed of 12 mm per second along the length of the beam. The X-Y table speed was chosen on the basis that there is a 5% overlap between the areas hit by consecutive laser pulses.

The rectangular beam of 2 mm x 1 mm was generated by a mask-imaging beam delivery system (Figure 5) that consisted of two telescope lenses (200 and 100 mm focal lengths), a turn mirror, and an image lens. The telescope lenses, set in a confocal configuration, were used to reduce the original beam size to half. The beam was passed through a rectangular slot in a copper aperture. The turning mirror was used to steer the rectangular beam on to the sample surface. The 100 mm focal length image lens was used to demagnify the aperture (object) size on the sample surface. The spot size was calculated using the demagnification ratio $M=O/I$, where O is the distance between the aperture and the image lens, and the distance between the image lens and the sample. The demagnification ratio in this setup was eight.

After laser treatment, the samples were characterized for crystalline structures by X-ray diffraction. Optical microscopy and scanning electron microscopy were used to examine the presence of solidification ripple structure as a function of pulse energy. Finally, the surface roughness was determined using a DekTak surface profilometer.

3. Finite Element Analysis of Temperature Distribution

In laser-material interactions during laser annealing, two processes take place. First is the absorption of laser light into a thin layer - on the order of nanometers - where the heat production takes place. The conversion of optical energy from the laser beam into thermal

energy involves excitation of electrons to states of higher energy levels through the absorption of photons. At 248-nm wavelength, the electrons are directly excited from states near Fermi energy to continuum states. Second, there is significant diffusive energy transport into the deeper parts of the material, where the electrons and lattice are in thermal equilibrium. While there have been several numerical and analytical models available to elucidate the physical mechanisms involved in the laser-material interaction, we resorted to a transient thermal conduction model to determine the temperatures spatially and temporally. During the laser pulse duration of 23 ns, thermal equilibrium between the lattice and the electron system was assumed. In addition, the following assumptions were made:

- The laser beam is normal to the surface
- The sample is initially at room temperature (300 K)
- The convective flow of heat is neglected.
- Thermal and physical properties are temperature-independent.

The FEM analysis was carried out using ANSYS package that essentially calculates the temperature at each node as a function of time from a heat balance equation based on the principle of conservation of energy. The ANSYS model can be run for a single laser pulse (23 ns) and also for the subsequent cooling period.

The governing transient heat flow equation is given by,

$$\frac{\partial^2 T}{\partial x^2}(x,t) - \frac{1}{\kappa}\frac{\partial T}{\partial t}(x,t) = -\frac{A(x,t)}{K} \qquad (1)$$

Where,

κ - Thermal Diffusivity (m^2/s)

K– Thermal Conductivity (W/m K)

x – Distance from the sample surface to the point where the temperature needs to be known (m)

t – Time elapsed (sec)

A (x, t) – Position dependent rate of heat absorption per unit time per unit volume (W/cm^3)

The heat absorption rate can also be expressed as,

$$A(x,t) = (1-R)I_0(t)\alpha \exp(-\alpha x) \qquad (2)$$

Substituting equation (1) in (2) yields

$$\frac{\partial^2 T}{\partial x^2}(x,t) - \frac{1}{\kappa}\frac{\partial T}{\partial t}(x,t) = -\frac{(1-R)}{K} I_0(t)\alpha e^{-\alpha x} \qquad (3)$$

Where,

R- Reflectivity of the surface

I_0 (t) - Time dependent laser intensity

The initial and boundary conditions are,

$$T(x,0) = T_0 \qquad (4)$$

$$T(0,t) = T_s \qquad (5)$$

T_0 and T_s are the initial and surface temperatures respectively.

If the laser intensity is assumed to be uniform over the area then the temperature predicted by analytical means becomes,

$$T(x,t) = T_0 = 2\frac{I_0}{K}\sqrt{t\alpha}\exp(\frac{-x^2}{4\alpha t}) - \frac{I_0 x}{K}(1 - erf\frac{x}{2\sqrt{t\alpha}}) \qquad (6)$$

But in the present case, the intensity is not really uniform over the entire area. So it becomes necessary to use a numerical method.

4. Results

Figure 6 shows the X-ray diffraction spectra of uncoated, sputter-coated and ELA-treated QC coating on aluminum substrates. The aluminum substrate generally exhibits three main peaks at 38°, 44° and 65°, but these peaks are hidden in the spectra of the sputter-coating except for the one at 65°. The laser-treated coating shows discrete crystalline peaks at 23°, 25°, 27°, 42°, 44°, 78° and 82°. The peak at 44° is interpreted as belonging to the underlying substrate but the peak intensity has increased due to the laser treatment. The highest intensity peaks appear to be the characteristic of the stable icosahedral phase as explained in the previous work [5].

X-ray diffraction analysis also revealed that there is a threshold pulse energy at which

Table 3. Threshold fluence for crystallization of QC coating

Substrate Material	Fluence (mJ/cm^2)
2024-aluminum	1000± 80
52100 steel	1250 ± 110
Ti-6Al-4V	1500±130

the phase transformation from amorphous to crystalline structure occurs. Table 3 shows the threshold energy fluence for crystallization of QC coatings in all three substrates. The crystallization phenomenon started only after the pulse energy reached the threshold for the given material. We believe that this threshold is directly related to the melting point and reflectance of the coating as well as thermal properties of the substrate. The small differences in threshold among the substrates are partly attributed to their thermal energy dissipation characteristics.

Figures 7(a) and (b) are the optical micrographs of aluminum samples treated with energy densities of 1 J/cm^2 (threshold) and 1.25 J/cm^2 respectively. Dendrite solidification structures along with unmelted regions (isolated zones) can be seen in Figure 7(a), suggesting the non-uniformities associated with melting at threshold energy fluence. In contrast, Figure 7(b) shows uniform dendrite structures indicating the evidence uniform melting and subsequent rapid solidification. Figures 7(c) and (d) show the surface of 52100 steel and Ti-6Al-4V samples respectively treated at 1 J/cm^2 where there is no evidence of melting because the energy fluence is well below threshold.

Figure 8 shows the increase in surface roughness with an increase in energy fluence. The rough surfaces generated in ELA are primarily attributed to the partial melting of the coating by the pulse energy, spatial inhomogeneties in the beam and microstructural non-uniformities in the coating. Surface micrographs revealed the ripple formation (Figure 9), a phenomenon associated with surface melting. We hypothesize that the evolution of surface roughness in ELA is a balance between roughening due to partial melting and smoothing processes due to the viscous flow of surfaces. Surface roughness data in conjunction with X-ray diffraction results confirmed that excimer laser crystallization is essentially a process of partial melting of a thin layer of coating and subsequent rapid, vertical solidification of the liquid phase to form a homogeneous layer. Irradiation with energy densities below threshold had negligible effects on the microstructure and surface roughness while irradiation at fluences much above threshold completely damaged the coating by pitting and delamination.

Table 4. Material Properties used in the FEM model

Material	**Thermal Conductivity (W/m K)**	**Density (kg/m^3)**	**Heat Capacity (J/kg K)**	**Reflectivity (%)**
$Al_{65}Cu_{23}Fe_{12}$	2	4000	500	NA
2024-Al	237	900	2700	27
Ti-6Al-4V	21.9	4540	520	53
52100 Steel	46.6	7810	475	36

The material properties used for the FEM analysis are presented in Table 4. An approximated Gaussian intensity distribution was applied to closely represent the energy

distribution of the laser beam, as the results of analysis are extremely sensitive to the intensity distribution [9]. Figure 10 compares the approximated Gaussian distribution used in our analysis to the actual Gaussian distribution and a uniform rectangular (or top-hat) distribution. The x-axis in the figure indicates the width of the laser beam on the coating surface (spot size along x-axis in mm), and the y-axis indicates the pulse power in watts. The intensity reaches maximum at the center of the pulse and reduces to zero on either side. The height of the peak depends on the irradiation energy which is varied for the three substrates. Figure 10 clearly illustrates why the triangular shape of the pulse approximates the Gaussian profile better than the uniform rectangular distribution. Even though the energy contained within the pulse is the same in both cases, they have significantly different effects on the temperature distributions.

For all three substrates, the maximum temperature attained (after irradiation for 23 ns) was in a very small region close to the material surface (Figures 11 to 13) and only a very thin melt layer is formed at the threshold. The melting temperature of QC coating is 835°C. The melt depth corresponding to threshold fluence was about 3 μm. It appears that in order for phase transition to occur, certain amount of melting is essential. For example, the surface temperature predicted for aluminum at an energy fluence of 0.75 J/cm^2 is 840°C, just a little over the melting point of the coating. However, there was no evidence of crystallization.

The melt depths computed for all three substrates are on the order of few micrometers as shown in Figure 14. The melt depths were computed at the center of the energy distribution where the crystallization effect is maxima. The temperature drops rapidly below the melt layer, minimizing the heat affected zone. Heat penetration did not occur into the

substrate material because of the controlled energy source (the laser) as well as the thermal insulation (2 W/m K) characteristic of QC. The total heat affected zone was found to be somewhere between 7 and 9 μm. Figure 15 shows the effect of energy fluence on the maximum temperature of QC coating deposited on aluminum substrate. The surface temperature increases almost linearly with the increase in energy fluence. The linearity is because the thermal properties of the coating were assumed not to change with the temperature. Even though the substrate material is expected to influence the heat transfer characteristics and thereby the temperature profile of the coating, the effect seems to be negligible. The reason for this is believed to be due to the extremely small melt depths encountered in this case.

Figure 16 presents the maximum temperature reached at the surface during laser irradiation. The time versus temperature plot is linear for all three materials. The molten material conducts the same amount of heat as the solid throughout the pulse width of 23 ns. The melt depth remains constant thereafter but still conducts heat away from the melt zone. Figure 17 shows the changes in melt depth with energy fluence for aluminum substrates; the trend is similar to the temperature plot providing further evidence that excimer laser can be used as a controlled heat source with extremely good accuracy.

5. Discussion

The discovery of stable quasicrystalline (QC) phases and an understanding of their structures led to a new group of engineering materials. Almost all the QC phases can be associated with crystalline phases containing icosahedrally packed groups of atoms. For

example, Al-Cu-Fe quasicrystals are found to be stable only after heat treatment at an elevated temperature [10]. The stable icosahedral phase begins to form only after the annealing temperature reaches 580°C [11]. The typical duration of the furnace annealing process is about 4 hours. The stability of the QC phases was found to be sensitive to small compositional variations, so that QC phases are commonly observed in association with other phases. But, annealing at temperatures between 800-900°C has been shown to restore the surface composition close to that of the bulk material [12]. Sordelet et al. [13] have shown that $Al_{65}Cu_{23}Fe_{12}$ contains both icosahedral and cubic phases with icosahedral being more predominant after annealing at temperatures over 500°C. Information from X-ray diffraction patterns in the present work indicate that laser annealing has been performed much above 700°C.

Laser surface treatment of thin films and coatings for the purpose of converting amorphous to crystalline structures is a growing industrial application. For example, excimer laser-induced crystallization of amorphous silicon to crystalline polysilicon is a key technology for high performance thin film transistor (TFT) devices, offering excellent resolution and brightness [14]. ELA is proven to be more flexible and economical than traditional furnace annealing [15]. The benefits of this process are several, the most important one being the ability to control the depth of heat penetration by rapid heating and cooling of the coated substrates. Due to the absence of thermal effects in the underlying substrate, it becomes possible to use any type of substrate.

Several research groups have used ELA for crystallizing various materials including Si [16], GaAs [17], Ge [18] and SiC [19]. In all these cases, the nanosecond-pulsed laser

irradiation deposits energy within a locally defined surface, causing the formation of a liquid phase and leading to nucleation and growth of crystalline regions during solidification of the molten layer [20]. However, the ELA crystallization process studied in depth [21-24] did not yield the conclusive evidence that the process always involved the formation of liquid phase. Furthermore, furnace annealing experiments revealed solid-phase crystallization of amorphous Si films where amorphous Si is directly converted to crystalline Si under isothermal conditions [25]. There is strong evidence that ELA of amorphous Si is essentially a transient process, involving melting and solidification of the Si films. The process involved rapid heating to melt the surface followed by cooling which takes only few nanoseconds [26]. The thermodynamically-distinct amorphous phase is energetically metastable relative to the crystalline phase. The driving force (free energy difference) for the transition of amorphous phase to the stable crystalline phase can be supplied through several mechanisms such as explosive crystallization and thermal shock. Explosive crystallization that occurs spontaneously at high temperatures consists of two steps: one is the rapid growth of liquid phase from the amorphous phase and two is the transformation from the liquid phase to the crystalline phase. The enthalpy release from the initial crystallization propagates the transformation of the remaining coating.

Interestingly, the process of explosive crystallization occurs in germanium over large depths at temperatures between 200-300°C. Si on the other hand needs much more rapid heating to initiate the process but is limited to shallow crystallization depths. Tsao and Peercy [27] suggested that explosive crystallization proceeds by nucleation of crystalline Si at a moving amorphous-liquid interface. Other models [28, 29] suggest that homogenous

nucleation of crystalline Si occurs during explosive crystallization at temperatures near the melting temperature of amorphous Si. Im et al. [30, 31] proposed the crystallization mechanism of amorphous Si in two major regimes (i.e., low- and high-energy-density regimes), and an important sub-regime (i.e., superlateral growth regime). These regimes were based on the dependence of grain size and the melt duration as a function of the incident energy density. The microstructures observed in the low-energy-density regime where the grain size increases with increasing energy density are shown to be associated with explosive crystallization followed by partial melting and regrowth of the film. Typically this regime is characterized by melt depth much smaller than the film thickness apart from smaller grain sizes. The complete melting of the film where substantial supercooling takes place before the onset of solidification via copious nucleation and subsequent growth of solids is the high-energy-density regime where the grain size is very small and is nearly independent of the incident energy density. The superlateral growth regime involves significant lateral growth before impingement with discrete regions of unmelted Si leading to the large grain size.

The situation in the low-energy-density regime is similar to that encountered in ELA of the amorphized Si surface layers, even though there is a disagreement about the process i.e., whether partial melting occurs before or after explosive crystallization. Studies revealed that under intense laser pulses above the threshold, amorphous Si can be partially melted and subsequently crystallized by a combination of upward and downward explosive crystallization steps [32-36]. Consistent with the above findings, the experimental results and the FEM model in the present work indicate that the liquid phase formation is essential

for the crystallization of QC. The crystallization of the amorphous QC is hypothesized to occur by explosive crystallization followed by partial melting and regrowth of the film at low energy fluences. The shallow melt depths provided the nucleation and growth of crystalline structures that have then propagated throughout the coating thickness. Even though crystallization appears to be stronger with increase in energy fluence (high-energy-density regime), there is a problem of substrate thermal damage and pitted surface leading to the conclusion that this regime may be better suited for conductive coatings rather than insulative coatings such as QC.

6. Conclusion

Excimer laser annealing of magnetron-sputtered, amorphous quasicrystalline coatings produced high hardness and toughness at the expense of increased surface roughness. X-ray diffraction, solidifications structure and ripple formation provided the evidence that the phase change from amorphous to crystalline involved the formation of liquid phase which also caused surface roughening. A 2-D finite element heat flow model validated the experimental data on threshold energy fluence for crystallization and pointed out conclusively that a thin melt layer has to be formed to obtain surface crystallization. The FEM model also predicted that the depth of melt layer required is on the order of micrometers.

Acknowledgements

The authors would like to acknowledge the financial support of U.S. National Science Foundation for this work, under SBIR grant SMI-0231722, "Laser Crystallization of Amorphous Sputter-Deposited Quasicrystalline Coatings on Conventional Engineering

Substrates", awarded to Engineered Coatings, Inc., in July 2003. We would also like to thank Matt Besser and Dan Sordelet of DOE Ames Laboratory and Frank Kustas of Engineered Coatings, Inc, for their continuous help and support by providing coated samples and also with the X-ray diffraction analysis.

References

[1] S. Kang, S. Dubois, and J. von Stebut, "Tribological properties of quasicrystalline coatings," J. Mater. Res. Vol. 8, No. 10, Oct. 93, 2471-2481.

[2] J. M. Dubois, P. Plaindoux, E. Belin-Ferre, N. Tamura, and D. J. Sordelet in: T. Fujiwara (Ed.), Quasicrystals, Proc. Of 6th Intl. Congr. On Quasicrystals, Tokyo, Japan, 1997, World Scientific, Singapore 1998, 733.

[3] D. Sordelet, M. Besser, and J. Logsdon, "Abrasive wear behavior of Al-Cu-Fe quasicrystalline composite coatings," Mater. Sci. Eng. A, 1998, 255, 54-65.

[4] P. Archambault and C. Janot, "Thermal Conductivity of Quasicrystals and Associated Processes," MRS Bulletin, Nov. 1997, 48-53.

[5] F. Kustas, P. Molian, A. Sadhu Kumar, M. Besser, and D. Sordelet, "Laser Crystallization of amorphous sputter-deposited quasicrystalline coatings," Surface & Coatings Technology, 188-189 (2004) 274-280.

[6] S. Urban, F. Falk, "Laser crystallization of amorphous Sic thin films on glass," Applied Surface Science, 184 (2001) 356-361

[7] K. Brendel, P. Lengsfeld, I. Sieber, A. Schöpke, N. H. Nickel, W. Fuhs, M. Nerding, and H. P. Strunk, "Excimer laser crystallization of amorphous silicon on molybdenum

coated glass substrates," Journal of Applied Physics, Vol 91(5) pp. 2969-2973 (March 1, 2002)

[8] V. Mikla, I. P. Mikhalko, and V. V. Mikla, "Laser-induced amorphous-to-crystalline phase transition in Sb_xSe_{1-x+}alloys," Matls. Sci. and Eng., B83 (2001), 74-78.

[9] M.R. Frewin and D.A. Scott, "Finite Element Model of Pulsed Laser Welding," Welding Research Supplement, (1999) 15s-22s.

[10] A. P. Tsai, "Metallurgy of Quasicrystals," MRS Bulletin, Nov. 1997.

[11] T. Grenet, F. Giroud, K. Loubet , A. Bergman, G. Safran , J. Labar, P. Barna , J.L. Joulaud, and M. Capitan, "Fabrication and transport properties of thin films of quasicrystals," Journal of Alloys and Compounds, 342, 2-6, (2002)

[12] Z.Shen, M.J.Kramer, C.J.Jenks, A.I.Goldman, T.Lograsso, D.Delaney, M.Heinzig, W.Raberg, and P.Thiel, "Crystalline surface structures induced by ion sputtering of Al-rich icosahedral quasicrystals," Physical Review B, Vol.58, No.15, October 1998.

[13] C.I.Lang, D.J.Sordelet, M.F.Besser, D.Schetman, F.S.Biancaniello, and E.J.Gonzalez, "Quasicrystalline coatings: Thermal evolution of structure and properties," J.Mater. Res., Vol.15, No.9, Sep 2000.

[14] D. Basting and H. Endert, "Excimer lasers for industrial microprocessing," The Industrial Physicist, September (1997), 40-44, American Institute of Physics

[15] J. Shida, S.Ishizaka, N.Kobayashi, and O.Kato, "Crystallization of a-Si Films by Excimer Laser Annealing Method," Japan Steel Works Technical Review (1997)

[16] J.S. Williams, and H.B. Harrison, in: J.F. Gibbons, L.D. Hess, and I.W. Sigmon (Eds.), "Laser and Electron-Beam Solid Interactions and Materials Processing," North-Holland, Amsterdam, (1981), 209.

[17] W. Wesch and G. Götz, "Rapid Annealing of ion-implanted GaAs," Phys. Stat. Sol., A 94 (1986), 745–765.

[18] F. Vega, J. Solis, J. Siegel and C.N. Afonso, "Delayed melting at the substrate interface of amorphous Ge films partially melted with nanosecond laser pulses," J. Appl. Phys. 88, 11 (2000), 6321–6326.

[19] A. Hedler, S. Urban, F. Falk, H. Hobert, and W. Wesch, "Excimer laser crystallization of amorphous silicon carbide produced by ion implantation," Applied Surface Science 205 (2003) 240-248

[20] P. Baeri, C. Spinella and R. Reitano, "Fast melting of amorphous silicon carbide induced by nanosecond laser pulse," Int. J. Thermophys. 20, 4 (1999), 1211–1221.

[21] D. Sands, P.H. Key, M. Schlaf, C.D. Walton, C.J. Anthony and M.J. Uren, "Optical characterization of lattice damage and recovery in ion-implanted and pulsed excimer laser irradiated 4H-SiC," Mater. Sci. Forum, 338–342 (2000), 655–658

[22] P.H. Key, D. Sands, M. Schlaf, C.D. Walton, C.J. Anthony, K.M. Brunson, and M.J. Uren, "Infra-red reflectivity of ion-implanted and pulsed excimer laser irradiated 4H-SiC," Thin Solid Films 364 (2000), 200–203.

[23] Y. Hishida, M. Watanabe, K. Nakashima and O. Eryu, "Excimer laser annealing of ion-implanted 6H-silicon carbide," Mater. Sci. Forum, 338–342 (2000), 873–876.

[24] H. Hobert, H.H. Dunken, S. Urban, F. Falk and H. Stafast, "Laser-induced changes of silicon carbon films studied by vibrational spectroscopy," Vibrat. Spectrosc., 29 (2002), 177–182.

[25] H. Kuriyama, T. Kuwahara, S. Ishida, T. Nohda, K. Sano, H. Iwata, H. Kawata,

S. Noguchi, S. Kiyama, S. Tsuda, S. Nakano, M. Osumi, and Y. Kuwano, "Enlargement of poly-Si film grain-size by excimer laser annealing and its application to high performance poly Si thin filmtransistor,"J. Appl. Phys. 31, 4550 (1991).

[26] Lee Kyung-ha, "A study on laser annealed polycrystalline silicon thin film transistors (TFTs) with SiNx gate insulator," (1998)

[27] J.Y.Tsao, and P.S.Peercy, "Crystallization instability at the amorphous-silicon liquid-silicon interface," Phys. Rev. Lett., 58, 2782 (1987)

[28] J.J.P.Bruines, R.P.M. Vanhal, H.M.J. Boots, A. Polman, and F.W. Saris, "Time-resolved reflectivity measurements during explosive crystallization of amorphous-silicon," Appl. Phy. Lett., 49,1160 (1986)

[29] K. Murakami, O. Eryu, K. Takita, and K. Masuda, "Explosive crystallization starting from an amorphous-silicon surface region during long-pulse laser irradiation," Phys. Rev. Lett., 59, 2203 (1987)

[30] J.S. Im, H.J. Kim and M.O. Thompson, "Phase transformation mechanisms involved in excimer laser crystallization of amorphous silicon films," Appl. Phys. Lett. 63, 1969 (1993)

[31] J.S. Im and R.S. Sposili, "Crystalline Si films for integrated active-matrix liquid-crystal displays," MRS bulletin, 39 (1996)

[32] A.G.Cullis, N.G.Chew, H.C Webber, and D.J.Smith, "Orientation dependence of high-speed silicon crystal-growth from the melt," J. Cryst. Growth, 68, 624 (1984)

[33] D.H.Lowndes, S.J.Pennycook, R.F.Wood, J.G.E.Jellison, and S.P.Withrow, Mater. Res. Soc. Symp. Proc. 100, 489 (1988)

[34] D.H.Lowndes, R.F.Wood, and J.Narayan, "Pulsed-laser melting of amorphous-silicon – Time resolved measurements and model calculations," Phys. Rev. Lett. 52, 561 (1984)

[35] M.O.Thompson, G.J.Galvin, J.W.Mayer, P.S.Peercy, J.M.Poate, D.C.Jacobson, A.G.Cullis, and N.G.Chew, "Melting temperature and explosive crystallization of amorphous silicon during pulsed laser irradiation," Phys. Rev. Lett., 52, 2360 (1984)

[36] W.Sinke and F.W. Saris, "Evidence for a Self-Propagating Melt in Amorphous Silicon upon Pulsed-Laser Irradiation," Phys. Rev. Lett., 53, 2121 (1984)

List of Figures

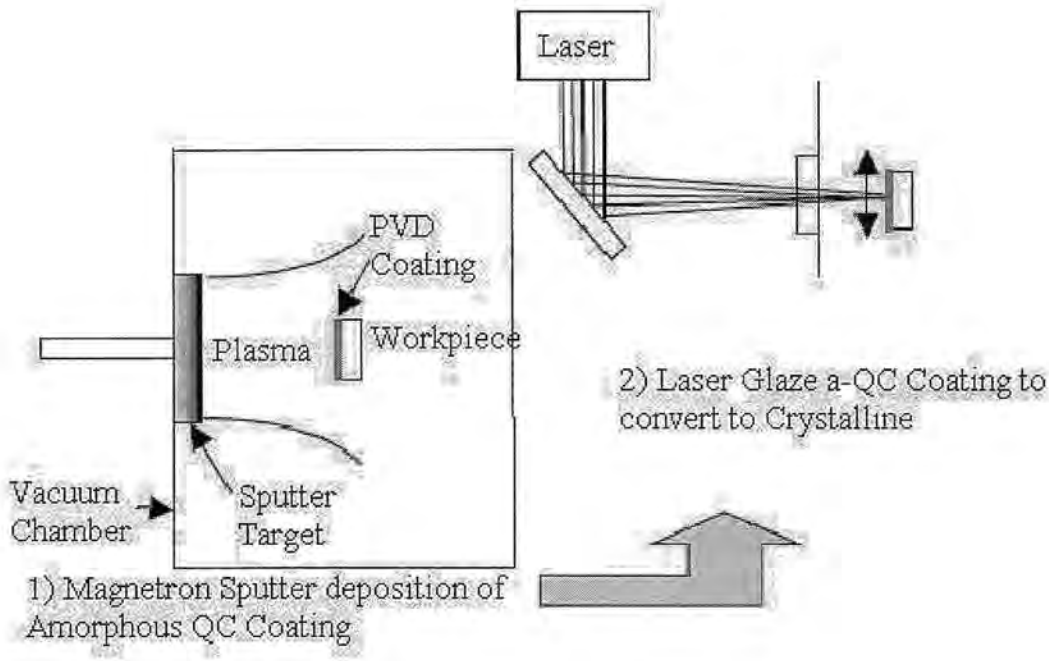

Figure 1. Magnetron sputtering and laser annealing to produce crystalline QC coatings

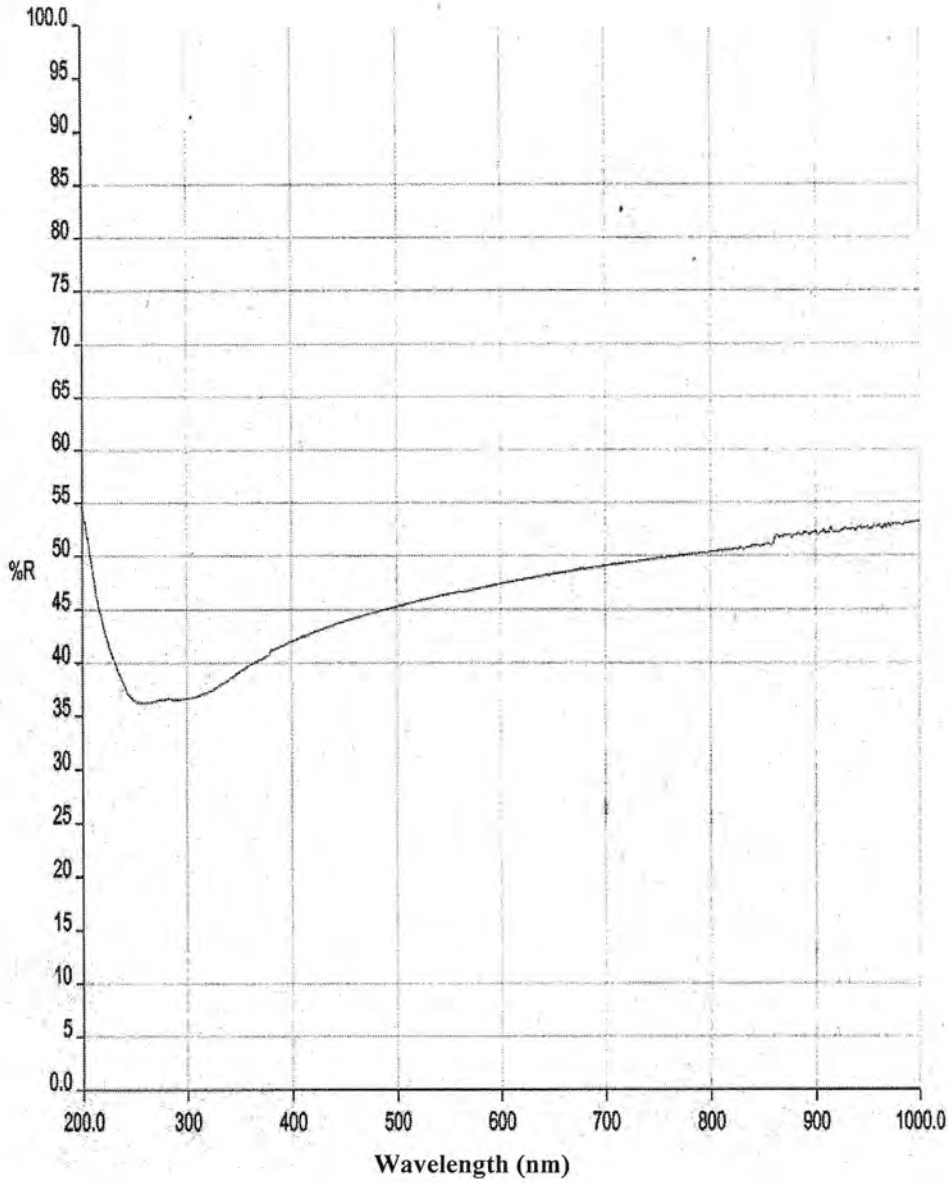

Figure 2. Reflectance plot for Steel between 200 and 1000 nm

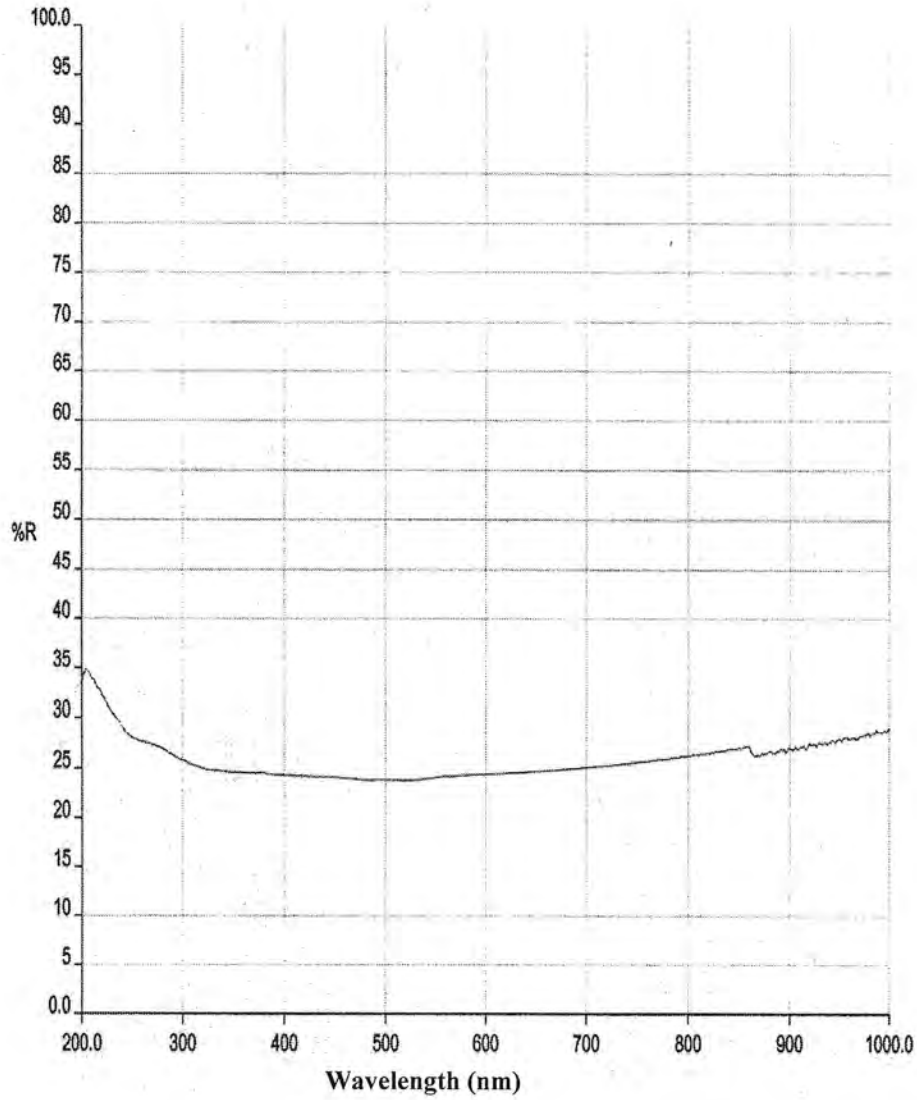

Figure 3. Reflectance plot for Aluminum between 200 and 1000 nm

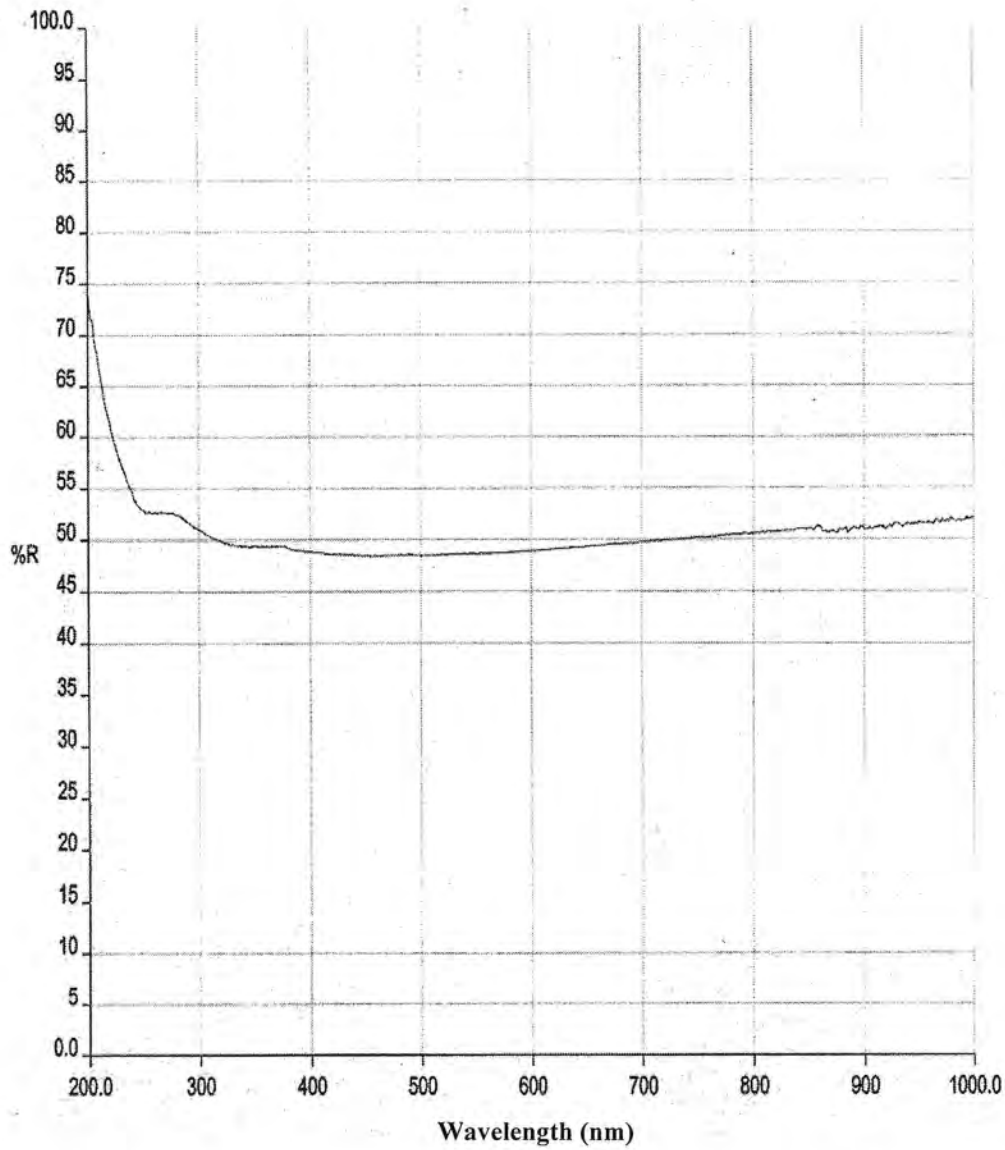

Figure 4. Reflectance plot for Titanium between 200-1000 nm

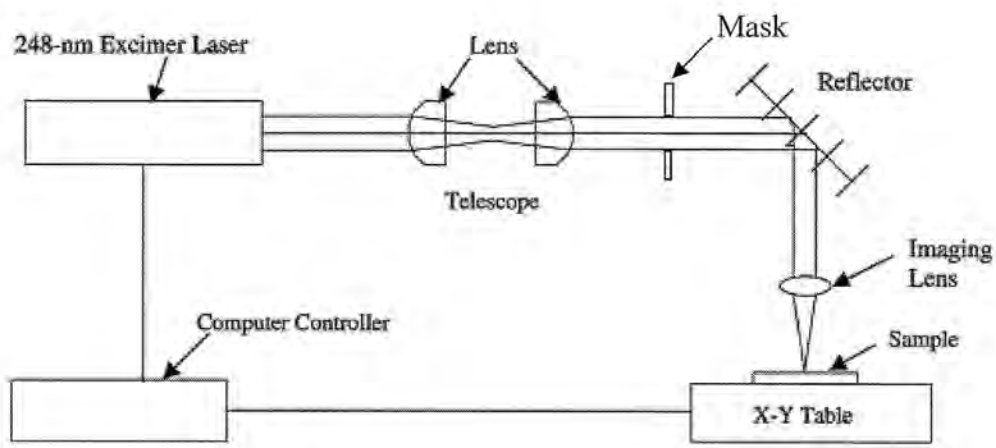

Figure 5. Schematic Representation of the experimental setup

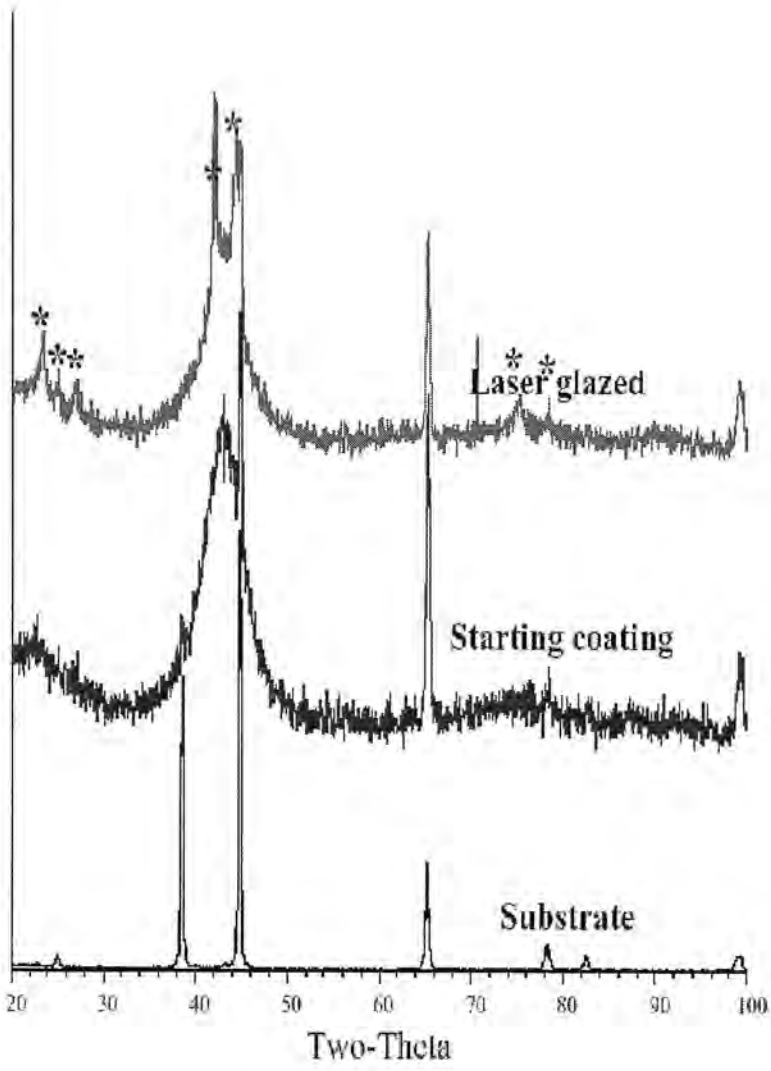

Figure 6. XRD spectra for QC coated on Al substrate

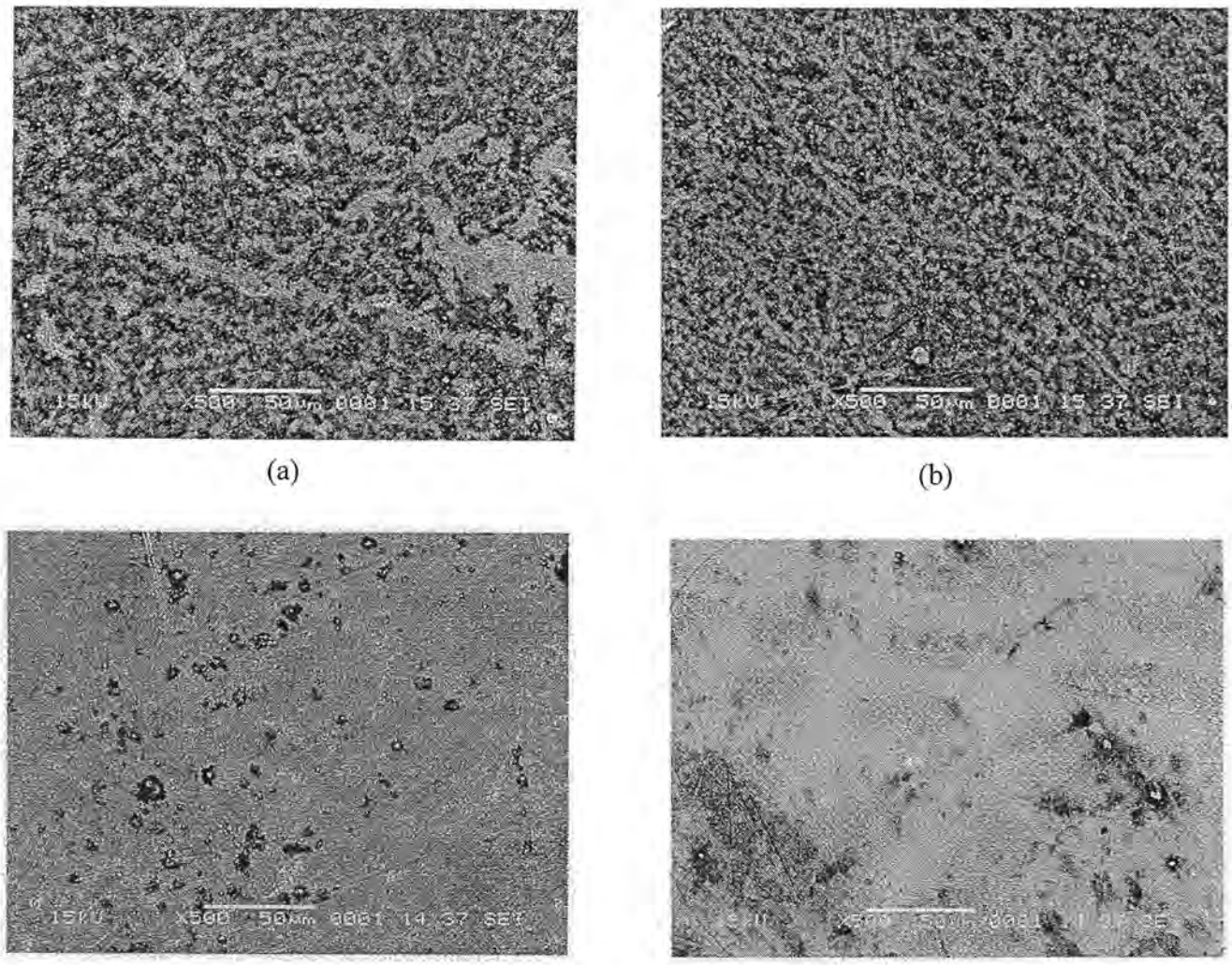

(a) (b)

(c) (d)

Figure 7. QC surface after laser treatment

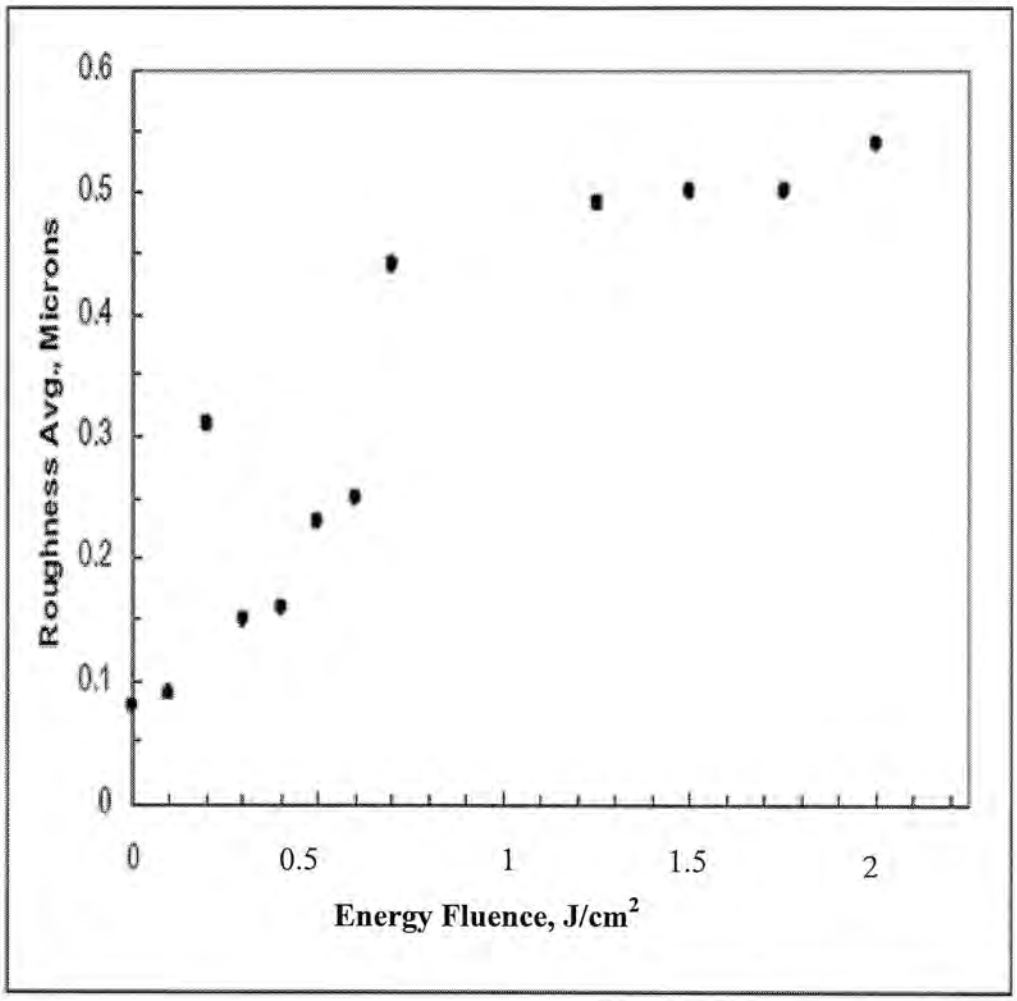

Figure 8. Roughness plot at various laser energy

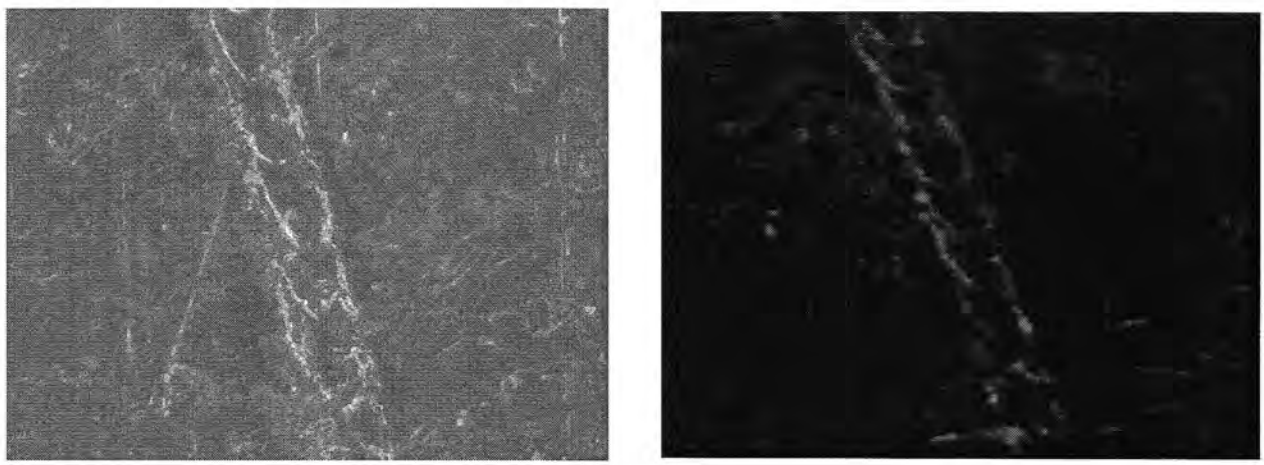

(a) (b)

Figure 9. Surface micrograph of a laser irradiated QC surface showing ripples

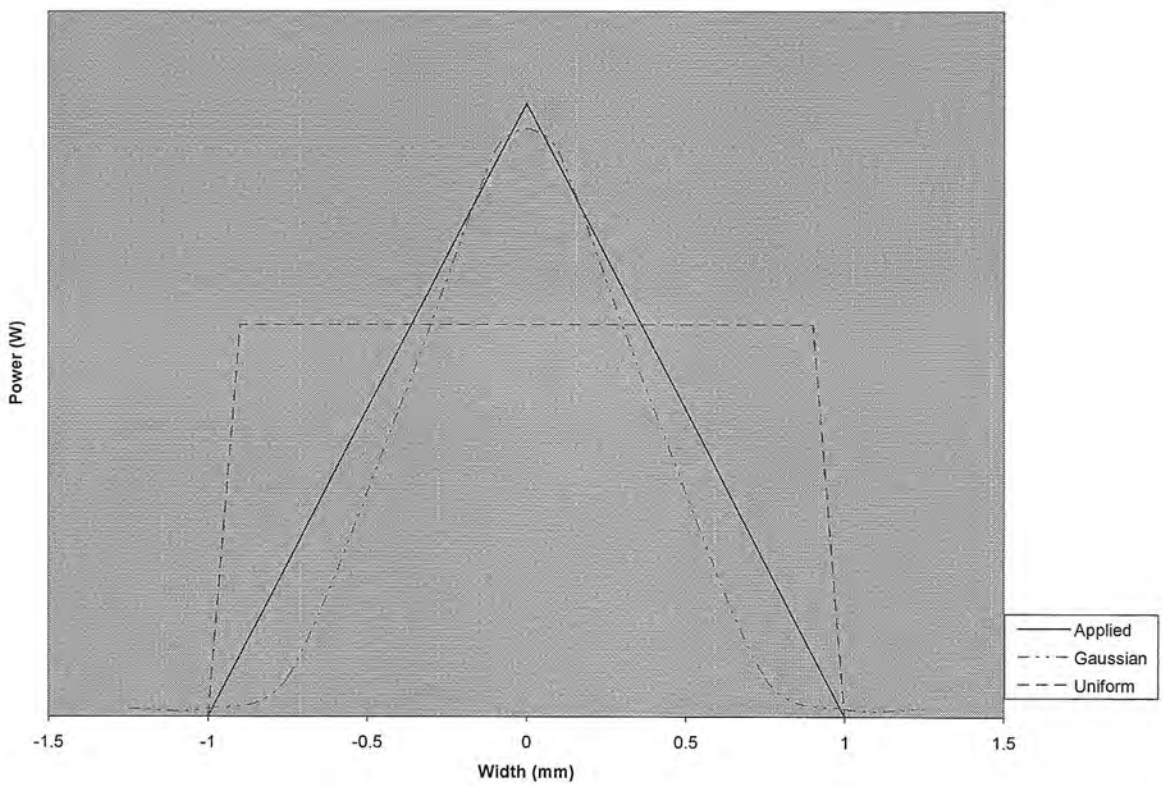

Figure 10. Surface load applied - Gaussian

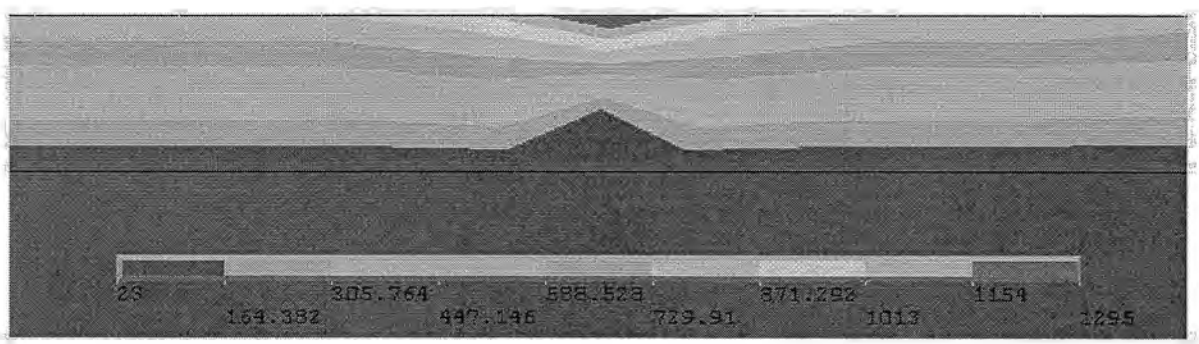

Figure 11. Temperature Profile for Aluminum Substrate

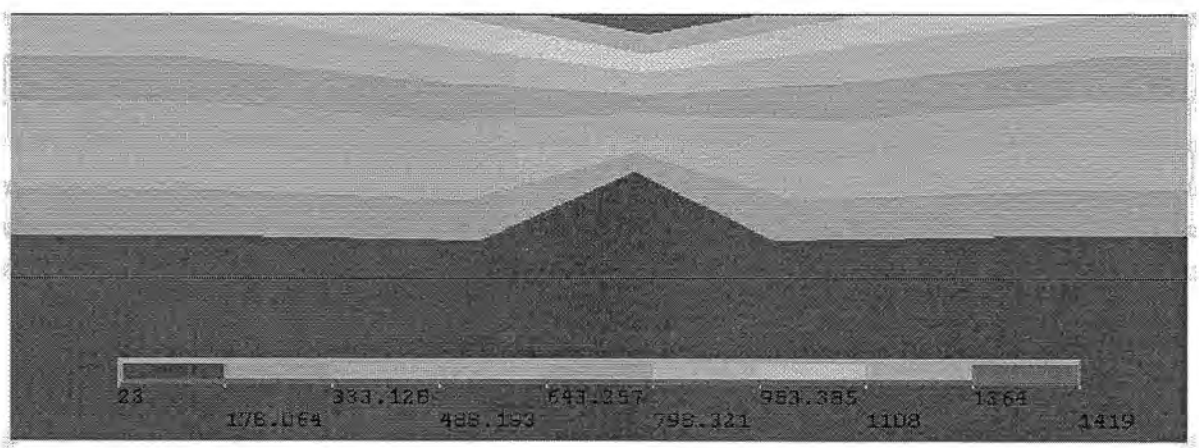

Figure 12. Temperature Profile for 52100 Steel Substrate

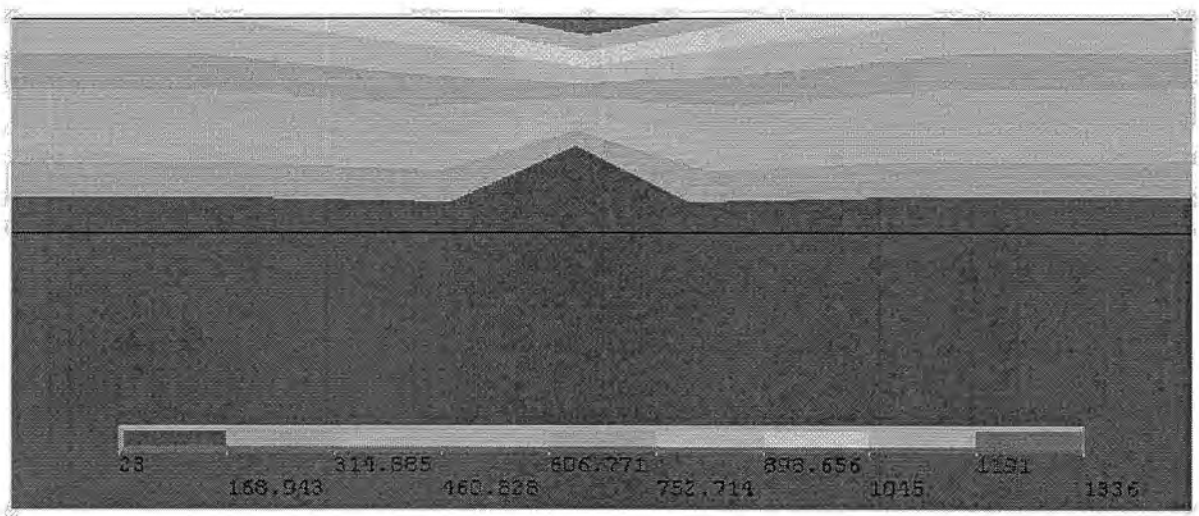

Figure 13. Temperature Profile for Titanium Substrate

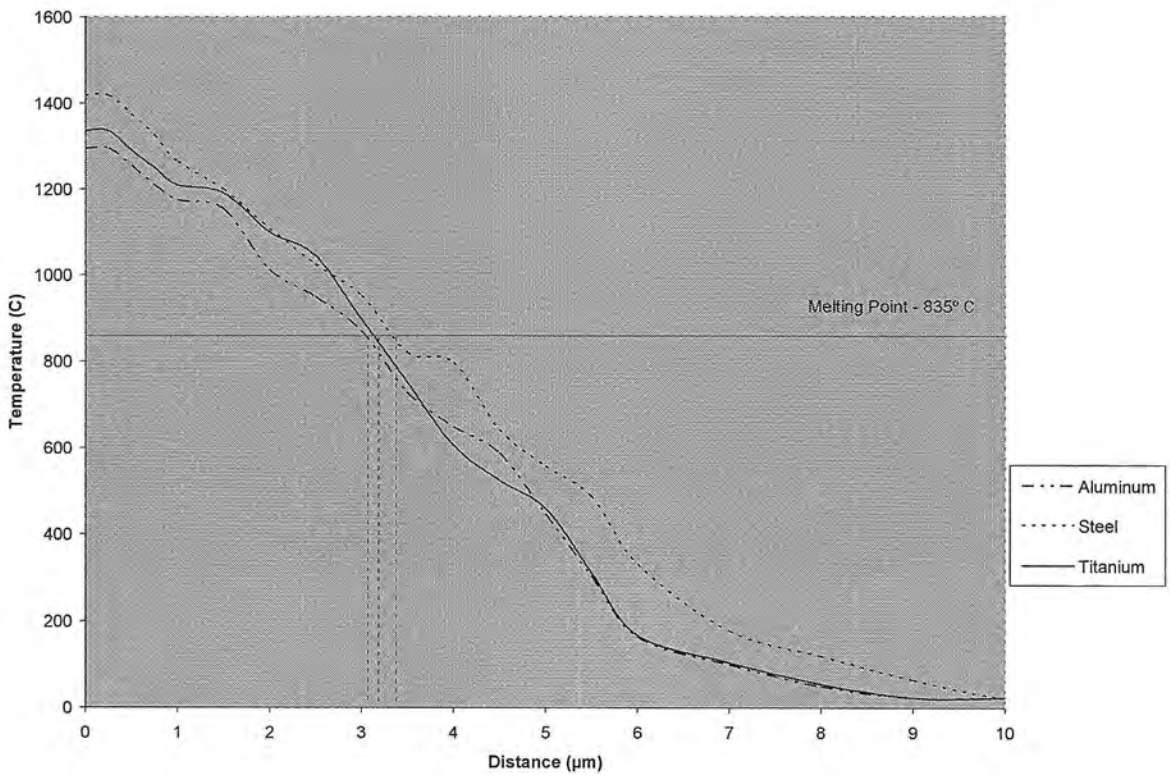

Figure 14. Melt Depth from ANSYS Model

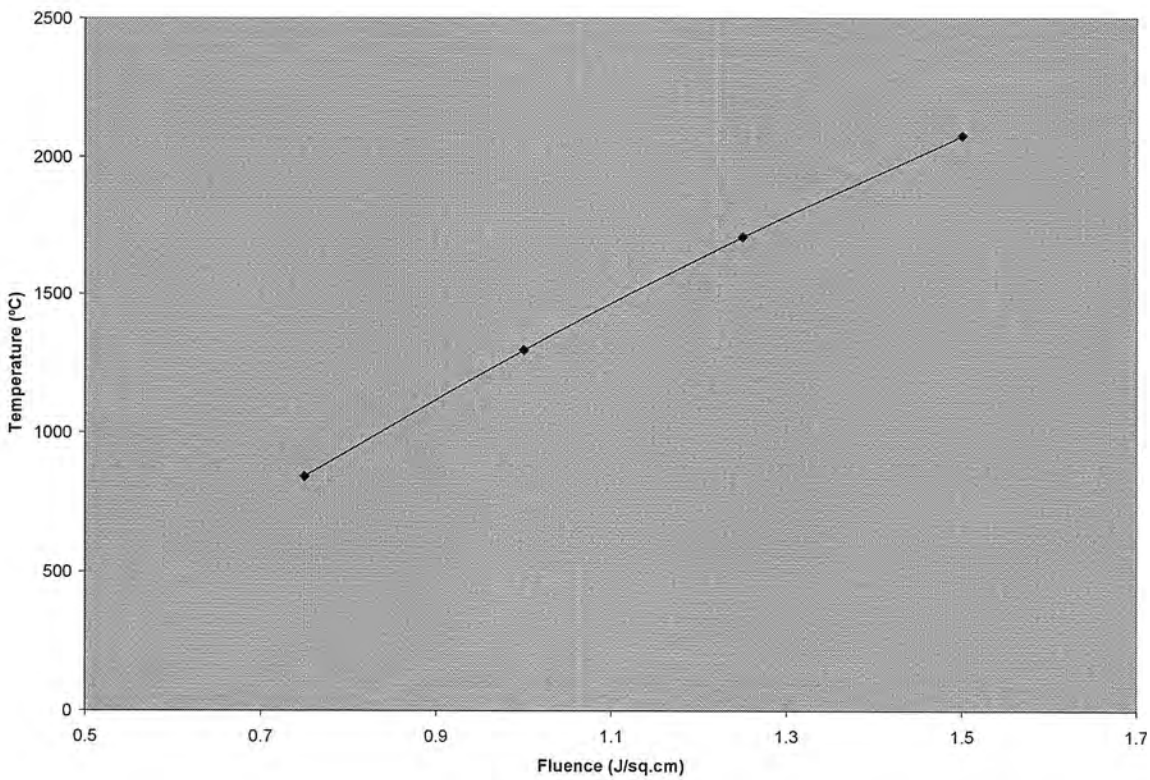

Figure 15. Maximum surface temperature at different fluences

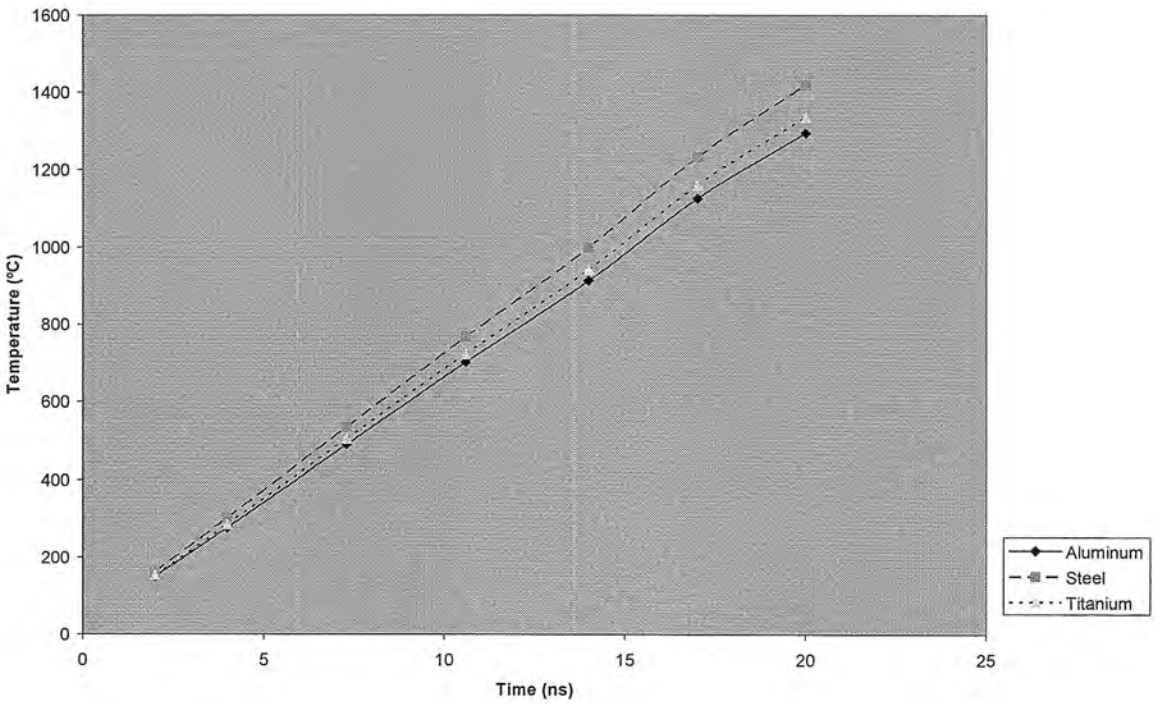

Figure 16. Temperature at different instants

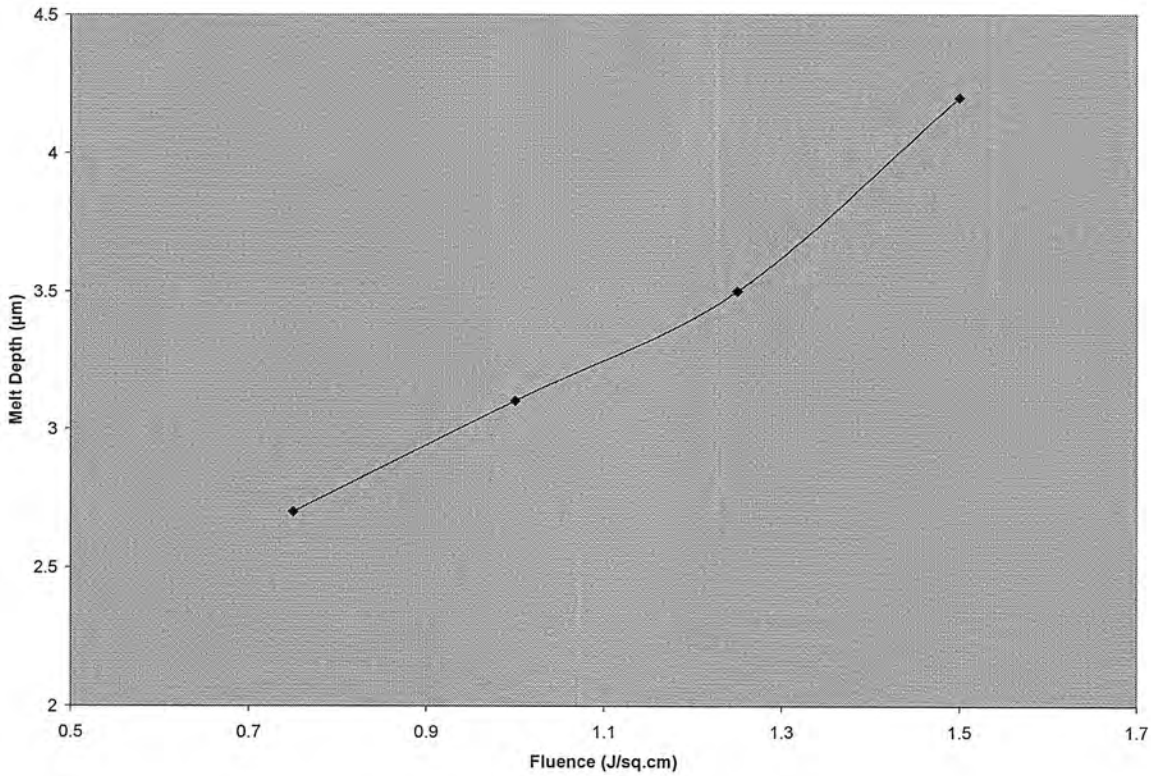

Figure 17. Melt Depths at different fluences

Chapter 4. Conclusions

Excimer laser crystallization of magnetron-sputtered quasicrystalline coatings deposited on conventional engineering substrates (52100 steel, 2024 Al and Ti-6Al-4V) was investigated as a function of laser parameters (energy fluence, pulse repetition rate, and beam scan rate) and amorphous layer thickness. The mechanical properties of coatings were determined. A finite element model was used to estimate the temperature distributions during pulsed laser heating of coatings.

Beneficial results were obtained in terms of crystalline structure, adhesion, friction, hardness and toughness. For example, the coefficient of friction was found to decrease by 25-40% depending on the substrate material and Rockwell C-Brale indentations showed absence of softening of the substrate.

Detrimental effect was observed in surface roughness. Experiments as well as FEM analysis revealed that the formation of a thin melt layer (3-3.5 μm) is essential for the phase transformation. However, the melt layer created the rippling phenomenon and caused an increase in surface roughness.

Recommendations for Future Research

The effect of beam profile and beam energy distribution on the surface roughness needs to be further examined. A flat, uniform, long beam that can be obtained by homogenizing the excimer laser beam will enable to minimize the temperature gradients in the melt layer and associated surface tension gradients, leading to smooth yet crystalline coatings.

Acknowledgements

This author would like to acknowledge the contributions of Dr. Frank Kustas of Engineered Coating, Inc, Dr. Dan Sordelet and Mr. Matt Besser of DOE, Ames lab for their continued support and collaboration throughout our research. The author would especially like to acknowledge his advisor Prof. Pal Molian whose continuous encouragement and guidance made this research possible.